THESIS

SPATIAL ARRANGEMENT OF STORMWATER INFILTRATION AFFECTS PARTITIONING OF SUBSURFACE STORAGE AND BASEFLOW TIMING

Submitted by

Benjamin Choat

Department of Civil and Environmental Engineering

In partial fulfillment of the requirements

For the Degree of Master of Science

Colorado State University

Fort Collins, Colorado

Spring 2019

Master's Committee:

Advisor: Aditi Bhaskar

Ryan Bailey
Michael Ronayne

ABSTRACT

SPATIAL ARRANGEMENT OF STORMWATER INFILTRATION AFFECTS PARTITIONING OF SUBSURFACE STORAGE AND BASEFLOW TIMING

Urban stormwater management is using distributed facilities that treat stormwater near where it falls at an increasing rate. These facilities are often designed to infiltrate water that would have previously been conveyed overland. By directing water that would have previously made it to receiving streams very quickly via overland flow into subsurface flow paths, the soil moisture, groundwater, and stream flow regimes are altered. While these alterations may have significant implications for urban watershed management, there remains a lack of knowledge about how spatial arrangements of infiltration focused facilities may affect catchment scale water-balances, including subsurface storage and streamflow. In particular, little focus has been given to relating site-scale behavior with catchment scale response. This project used a physically-based numerical model, ParFlow, to investigate the relationships between spatial arrangements of infiltration facilities, subsurface partitioning of water between unsaturated and saturated zones, and baseflow response duration and timing. Our findings show that more spatially distributed infiltration facilities, as compared to spatially-clustered infiltration facilities, encourage greater unsaturated zone storage, less saturated zone storage, and more total subsurface storage in scenarios where surface ponding is not severe. Depth to water table beneath infiltration facilities was found to be the main driver of observed differences in partitioning of subsurface storage. In our lowest conductivity soil, silt, severe groundwater mounding was observed at steady-state with significant surface ponding. In a catchment with high permeability and diffusivity, baseflow response to precipitation was delayed in the clustered infiltration scenario compared to the distributed scenario. The clustered scenario resulted in more baseflow after longer inter-event durations but lower baseflow between sequential precipitation events with short inter-event durations. In the same catchment, antecedent moisture was shown to amplify sensitivity of baseflow response to clustered infiltration spatial arrangement. These

results can be used to help guide decisions about spatial locations of stormwater infiltration facilities to meet urban watershed management goals such as increasing plant available water, increasing aquifer recharge, producing more consistent or dynamic baseflow, and quicker or more delayed baseflow responses to precipitation.

TABLE OF CONTENTS

Chapter 1: Introduction

Flow is considered the master variable for stream function. Managing flow regime will minimize or encourage recovery from altered stream functional states (Poff et al. 1997). Urbanization impairs stream health by altering natural flow regimes, water quality, geomorphology, and ecological function and structure (Walsh et al. 2005). Sealing of pervious areas and direct conveyance of stormwater to streams are the primary drivers of flow regime changes occurring with urbanization. Conveyance-based stormwater management increases flashiness of stream hydrographs, decreases time to peak flow, increases magnitude of peak flow, increases hydrograph recession rates, and alters catchment-scale water balances (Jefferson et al. 2017; Walsh et al. 2005). Water that once would have infiltrated into the ground and slowly discharged as baseflow, defined here as groundwater-fed streamflow, is shifted to runoff.

Many approaches to reduce peak flows in urban streams use stormwater detention. Yet, even when peak flows are effectively managed, degradation of stream geomorphology, water quality, and stream ecology are still observed if the rest of the flow regime remains in an altered state (Poff et al. 1997; Walsh et al. 2005; Jefferson et al. 2017). Furthermore, urban-induced changes in water yield and baseflow can also affect water availability for downstream users or cause flooding of subsurface infrastructure (Endreny and Collins 2009; Bhaskar et al. 2016). Newer forms of stormwater management (called green infrastructure or low impact development) therefore seek to meet watershed management goals by incorporating harvest or infiltration of stormwater. Distributed harvest or infiltration stormwater control measures (SCMs) reduce the volume of stormwater entering urban streams. These approaches can be effective at reducing peak flows for small- to medium-sized precipitation events (Jefferson et al. 2017; Loperfido et al. 2014; James and Dymond 2012; Hood, Clausen, and Warner 2007; Lim and Welty 2017). Maintaining the natural flow regime during development is theoretically possible if appropriate volumes of water are harvested and infiltrated using SCMs (Askarizadeh et al. 2015). Harvested water manipulates catchment water balances by increasing evapotranspiration (ET) or trans-basin export of stormwater (Askarizadeh et al. 2015). Infiltrated water manipulates catchment water balances by routing stormwater into the subsurface, increasing subsurface storage, which in turn drives catchment outputs via subsurface flow and baseflow of local streams (Bhaskar et al. 2016; Bhaskar, Hogan, and Archfield 2016; Hamel, Daly, and Fletcher 2013; Hamel and Fletcher 2014; Newcomer et al. 2014; Jefferson et al. 2017; Price 2011). Harvesting stormwater decreases subsurface storage and baseflow, whereas infiltration of stormwater may be pursued as a way to counteract reduced recharge caused by impervious surfaces and increase baseflow (Jefferson et al. 2017; Askarizadeh et al. 2015).

Optimizing urban stormwater infiltration to meet management goals for baseflow and groundwater recharge requires consideration of both anthropogenic and natural catchment characteristics. Anthropogenic alterations to recharge and groundwater elevation in urban settings are induced by changes in effective imperviousness (Voter and Loheide 2018; Jefferson et al. 2017), spatial arrangement of impervious surfaces (Endreny and Collins 2009), vegetative cover, water imports and exports (Lerner 2002), and leaky water infrastructure (Bhaskar et al. 2015).

Natural catchment characteristics driving groundwater elevation in urban settings include climate, physiography, and soil type. Climatic factors largely govern the volume of water available for recharge in urban areas. These factors include atmospheric demand and ET (Miles and Band 2015; Bhaskar et al. 2016; Thomas, Behrangi, and Famiglietti 2016), and typical event intensity, duration, and frequency (Eger, Chandler, and Driscoll 2017; Thomas, Behrangi, and Famiglietti 2016; Lim and Welty 2017; Chui and Trinh 2016). Physiographic characteristics such as topography (Miles and Band 2015; Bhaskar et al. 2016) and geology (Bhaskar et al. 2016; Thomas, Behrangi, and Famiglietti 2016) are also major factors in resulting urban water table elevations. Soil type has been used as an all-encompassing characterization of many soil parameters by some (Thomas, Behrangi, and Famiglietti 2016; Bhaskar et al. 2016), while others have identified specific attributes of soil type such as saturated hydraulic conductivity (Eger, Chandler, and Driscoll 2017; Chui and Trinh 2016; Endreny and Collins 2009) and porosity (Thomas, Behrangi, and Famiglietti 2016) that drive urban recharge and groundwater elevations. Infiltration rate (Miles and Band 2015; Göbel et al. 2004; Chui and Trinh 2016) and antecedent moisture content (Endreny and Collins 2009; Chui and Trinh 2016; Loperfido et al. 2014; Eger, Chandler, and Driscoll

2017; Hood, Clausen, and Warner 2007) have also been identified as drivers of stormwater recharge, although these are time-variable functions of soil type (saturated hydraulic conductivity, soil porosity, residual soil moisture, soil moisture retention curve) and storm characteristics (rainfall intensity and duration, inter-event duration, etc.). Therefore, we consider the primary natural drivers of recharge as climate, physiography, and soil type. Baseflow is sourced from groundwater recharge and therefore is sensitive to the same drivers as recharge. In addition, there are some factors that directly affect baseflow and not recharge, such as subsurface flow path length, hydraulic gradient between the riparian aquifer and stream, and streambed permeability (Hamel, Daly, and Fletcher 2013; Price 2011).

Soil type and associated unsaturated zone behavior mediates the translation of infiltration to recharge, but is commonly ignored due to difficulty in direct observations and computational demand required for unsaturated flow simulations (Healy 2010, sec. 3.3). Approaches ignoring unsaturated zone behavior may directly apply precipitation to recharge, and treat the movement of stormwater infiltration to baseflow as a saturated flow problem characterized by saturated hydraulic conductivity and specific yield. Even when stormwater modeling considers subsurface dynamics, simplified 1-d approximations for infiltration are typically implemented, such as Green-Ampt (e.g., SWMM; Rossman 2015). The Green-Ampt (Heber Green and Ampt 1911) approach assumes 1-d flow in a semi-infinite domain (i.e., no interaction with a lower boundary condition), whereas recharge, by definition, has a lower boundary condition of saturation. If a 1-d approximation is used, infiltration SCMs (I-SCMs) arranged close together vs. further apart receiving the same volume of stormwater for infiltration would lead to nearly identical outcomes for watershed-scale recharge, subsurface storage, and baseflow. However, in a 3-d setting, due to horizontal flow and storage in the unsaturated zone, the arrangement of I-SCMs, and not only the volume of stormwater received, may affect recharge, subsurface storage, and baseflow. Ignoring or using 1-d simplifications of unsaturated zone behavior and describing soils using saturated hydraulic conductivity and specific yield may be reasonable in certain situations under appropriate temporal and spatial scales, but over shorter time periods such as days or hours, and over smaller areas with non-uniform infiltration, such as small urbanized catchments or hillslopes, unsaturated zone dynamics likely play a significant role in modulating how infiltration is translated to recharge and baseflow (Woods, Sivapalan, and Robinson 1997; Staudinger et al. 2019) Elucidating the relationships between unsaturated zone storage, saturated zone storage, recharge, baseflow, and the distributed nature of stormwater infiltration therefore requires use of a variably-saturated three-dimensional approach.

Low impact development offers an opportunity to manipulate some of the catchment characteristics driving recharge and baseflow including effective imperviousness, spatial arrangement of impervious surfaces, subsurface flow path length, and soil types. Managing total imperviousness may be limited by urban growth development pressures and policies or existing development density. On the other hand, spatial arrangement of I-SCMs (i.e., clustered vs. distributed) may be varied while keeping the same development density. Altering the spatial arrangement of SCMs can lead to reductions in effective imperviousness while maintaining the same total imperviousness (Lim and Welty 2017; Gilroy and McCuen 2009) and it may be possible to manipulate subsurface flow path lengths affecting baseflow timing and magnitude. However, we currently lack the knowledge to predict the effect of spatial arrangement of I-SCMs on baseflow, preventing informed stormwater network design that aims to manage the entire flow regime. Previous work connecting I-SCMs, groundwater recharge, and baseflow has been observational (Jefferson et al. 2017; Bhaskar, Hogan, and Archfield 2016; Bhaskar et al. 2018). In observational studies, the location of I-SCMs cannot be moved while keeping all other catchment characteristics the same, and therefore observations are limited to comparisons between watersheds with different I-SCM arrangement as well as differences in other catchment characteristics such as soil type. With physically-based numerical modeling, controlled experiments can be undertaken to isolate the effect of spatial arrangement of stormwater infiltration on recharge and baseflow from the effect of other factors. In particular, distributed modeling approaches have the ability to capture physical catchment characteristics and spatially explicit features to which baseflow response is sensitive (Hamel et al., 2013). Previous work using distributed models to connect I-SCMs with groundwater or baseflow response has been limited to site-scale or local-scale groundwater response rather than catchment-scale streamflow response (Endreny and Collins, 2009; Newcomer et al., 2014; Li, et al., 2017). We hypothesized that focused, discrete spatial infiltration, when spatially distributed over larger areas, leads to larger horizontal hydraulic gradients beneath I-SCMs resulting in significant lateral subsurface flow, decreasing episodic recharge and baseflow and increasing storage.

Our overarching goal is to evaluate how baseflow responds to distributed stormwater infiltration. To understand the dynamics of this relationship we ask the following questions:

(1) How does spatial arrangement of I-SCMs affect total subsurface storage, partitioning of storage between unsaturated and saturated zones, and episodic baseflow recession and timing?

(2) How are drivers of flow beneath infiltration facilities different between spatial arrangements?

(3) How do the effects of spatial arrangement of I-SCMs on subsurface storage and baseflow vary among soil types?

We executed a series of idealized simulations of distributed and clustered I-SCM spatial arrangements implemented on three native soil types using an integrated surface-subsurface watershed model to answer these questions.

Chapter 2: Methods

2.1 General Methodology

We used a physically-based watershed model, ParFlow (Kollet and Maxwell 2006; Ashby and Falgout 1996; Maxwell 2013; Jones and Woodward 2001), to simulate idealized catchments with two spatial arrangements of I-SCMs. ParFlow models surface and subsurface flow by solving a kinematic wave approximation for overland flow implicitly coupled to Richards' equation, allowing for dynamic groundwater surface water interactions (Kollet and Maxwell 2006). ParFlow is a fully distributed, integrated surface-subsurface cell-centered finite-difference watershed modeling code designed for parallel computation. We chose ParFlow because it allows for physically-based representations of the hydrologic processes of infiltration, subsurface flow, and groundwater-surface water interactions, key to addressing our questions, whereas other models simplify one or more of these processes.

2.2 Model Domain Development

To isolate effects of spatial arrangement of I-SCMs, we simulated an idealized wedge-shaped urban catchment (Figure 1). The surface area of the domain was 0.25 km^2 (0.5 km x 0.5 km) with a uniform thickness of 28 m. The computational grid was discretized to 5 m x 5 m in the horizontal resulting in 10,000 cells per layer. Variable vertical discretization was implemented with 14 layers representing a total thickness of 28 m, resulting in a total of 140,000 cells for the model domain. From top to bottom, the thickness of each layer of cells was 0.5 m, 0.5 m, 1 m, 1 m, 1 m, 1 m, 1 m, 1 m, 2 m, 2 m, 2 m, 5 m, 5 m, and 5 m. We used a terrain-following grid such that the angle of each surface cell was applied to all subsurface cells located below it (Maxwell 2013).

We developed a digital elevation model (Figure 1) from which slopes were attained as the input for ParFlow. Then we modified a slope development routine ((Barnes, Welty, and Miller 2016)) to set slopes of I-SCM cells to zero in both directions and stream cell slopes to zero in the direction perpendicular to streamflow. By assigning slopes of zero at I-SCM cells, water was only able to leave those cells through infiltration or evapotranspiration (ET). Specifying cells representing the stream to have zero slopes in the direction perpendicular to flow forced all flow to exit the domain at the outlet cell. Other than at I-SCMs resulting slopes parallel to streamflow (in the x-direction) were constant at 0.1%. Slopes perpendicular to streamflow (in the y-direction) were 0% in the row of stream cells, 25% in the cells adjacent to the stream (riparian cells), 15% along the row of impervious cells closest to the stream, and other than at I-SCMs, 5% throughout the rest of the domain.

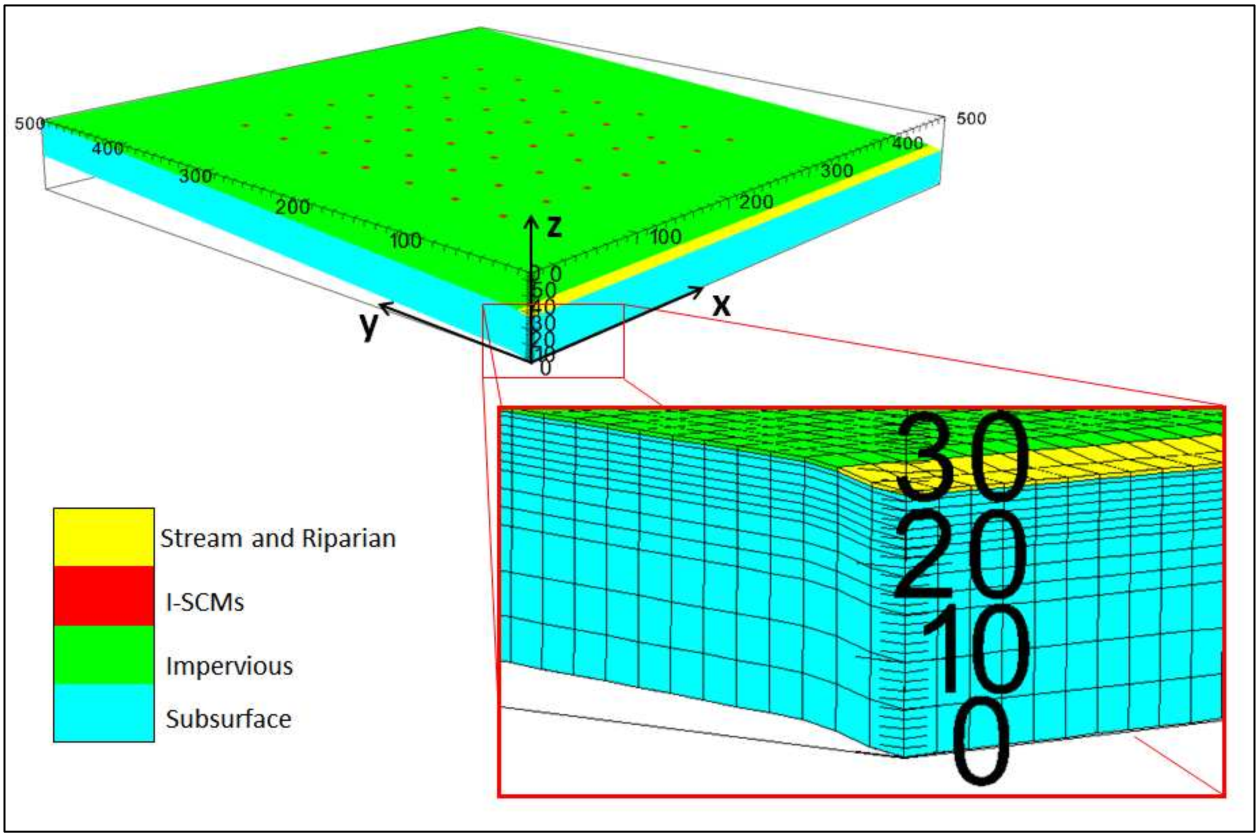

Figure 1. Model domain with distributed I-SCM arrangement and cells colored according to regions of the domain. Cutaway highlights terrain-following computational grid with variable vertical discretization. The stream outlet cell is at (0, 0, 28 m).

2.3 Physical Domain Properties

Representing a densely urbanized hillslope, all surface cells were defined as impervious except for I-SCM cells, riparian cells, and stream cells (Figure 1). Impervious surfaces were represented by the top cell layer (0.5 m). I-SCMs were specified to be the top 1 m (two cell layers) of the domain. Stream and riparian cells were assigned a Manning's roughness coefficient of 4.05e-7 d/m$^{1/3}$ (corresponding to

0.035 s/m$^{1/3}$ for natural streams and floodplains) and impervious cells a roughness coefficient of 3.5e-7 d/m$^{1/3}$ (corresponding to 0.026 s/m$^{1/3}$ for a rougher surface than impervious surfaces since no flow obstacles were included).

Subsurface properties were assumed to be homogeneous and isotropic. Three different soils, silt, loamy sand, and sand, were simulated using saturated hydraulic conductivity (Ks) and van Genuchten parameters ($\boldsymbol{\alpha}$, n, θs, θr) obtained from ROSETTA (Schaap, Leij, and van Genuchten 2001) (Table 1) and a van Genuchten relative permeability function (van Genuchten 1980) within ParFlow (Maxwell et al., 2016). We applied constant specific storage in all scenarios (9.82e-4 m^{-1}). Unsaturated parameters of impervious surface cells were based on concrete (Gupta, Singh, and Ranaivoson 2004) and saturated hydraulic conductivity of impervious cells was based on measurements on fractured pavements (Wiles and Sharp Jr 2008). I-SCM cells were assumed to have physical properties of sand.

To illustrate how these soil types relate to more commonly used aquifer parameters, we estimated the corresponding specific yield and aquifer diffusivity. Specific yield (Sy) was estimated as the difference between saturated soil moisture (θs) and residual soil moisture (θr). While hydraulic conductivity defines the ease with which water flows through porous media and drives the velocity of groundwater movement, the timing of streamflow response to pressure perturbations in the hydraulic conditions far from the stream (such as groundwater pumping, or in our case, groundwater recharge from stormwater) is driven by aquifer diffusivity. Aquifer diffusivity defines the rate of horizontal propagation of hydraulic stresses, and for an unconfined aquifer is defined as transmissivity divided by Sy (Barlow and Leak, 2012). We calculated aquifer diffusivity, Ds [m^2/d], per aquifer thickness, b [m], as Ks divided by Sy (Table 1). After transient simulations, we used resulting mean aquifer thickness to calculate aquifer diffusivity as Ds/b*b for loamy sand and sand and both I-SCM arrangements.

Table 1. Subsurface properties of saturated soil moisture θs [-], residual soil moisture θr [-], van Genuchten α [1/m], van Genuchten n [-], saturated hydraulic conductivity Ks [m/d], specific storage for three soil types, and impervious cells; specific yield Sy [-] and aquifer diffusivity Ds [m/d] of three soil types.

Textural Class	θr	θs	α [1/m]	n	Ks [m/d]	Sy	Ds/b [m/d]
silt	0.05	0.489	0.66	1.68	0.44	0.44	1.00
loamy sand	0.049	0.39	3.5	1.75	1.05	0.34	3.07
sand	0.053	0.375	3.5	3.18	6.42	0.32	19.96
impervious	0.094	0.23	1.9	1.59	1.00E-03	-	-

2.4 Boundary Conditions

Boundary conditions along all subsurface boundaries (four sides and bottom) were no-flow boundaries and an overland flow boundary condition was implemented for the surface boundary, allowing spatially-variable boundary conditions to be applied to individual surface cells (OverlandFlowPFB;(Kollet and Maxwell 2006)). Annual precipitation was selected to represent a moderately humid climate (100 cm/yr). Since streams are more likely to be gaining in humid areas, we expected a humid area to offer the most opportunity for spatially distributed I-SCMs to be effective at managing baseflow. Precipitation was applied to riparian and stream cells at the steady-state or transient precipitation rate (discussed below). We used a below average ET to precipitation ratio (ET/P) of 0.4 (Reitz et al., 2017) since development is likely to decrease ET, resulting in an annual ET of 40 cm/yr. This ET rate was translated to a volume across the entire domain, and then was applied equally to all I-SCM, riparian, and stream cells (i.e., impervious areas did not have ET).

Two spatial arrangements of I-SCMs were simulated and are referred to as clustered and distributed. Both arrangements had 49 total SCMs centered around the same location, the center of the impervious area. Each I-SCM was represented as the size of a grid cell (5 m x 5 m or 25 m^2). For the clustered scenario, 49 I-SCMs were distributed over 169 grid cells (49 SCMs/0.00423 km^2 or 11,597.6 SCMs/km^2) while 49 I-SCMs were distributed over 3,025 grid cells in the distributed scenario (49 SCMs/0.0756 km^2 or 647.9 SCM/km^2) in 7 x 7 gridded patterns (Figure 2). Overland routing of stormwater was not the focus of this study and the numerical experiment was facilitated by equal stormwater volumes reaching each I-SCM. Therefore, all rainfall over the impervious area was routed directly to I-SCM cells, such that each I-SCM received an equal volume of stormwater. This routing was carried out as a pre-processing step and was input into ParFlow using the OverlandFlowPFB surface boundary condition.

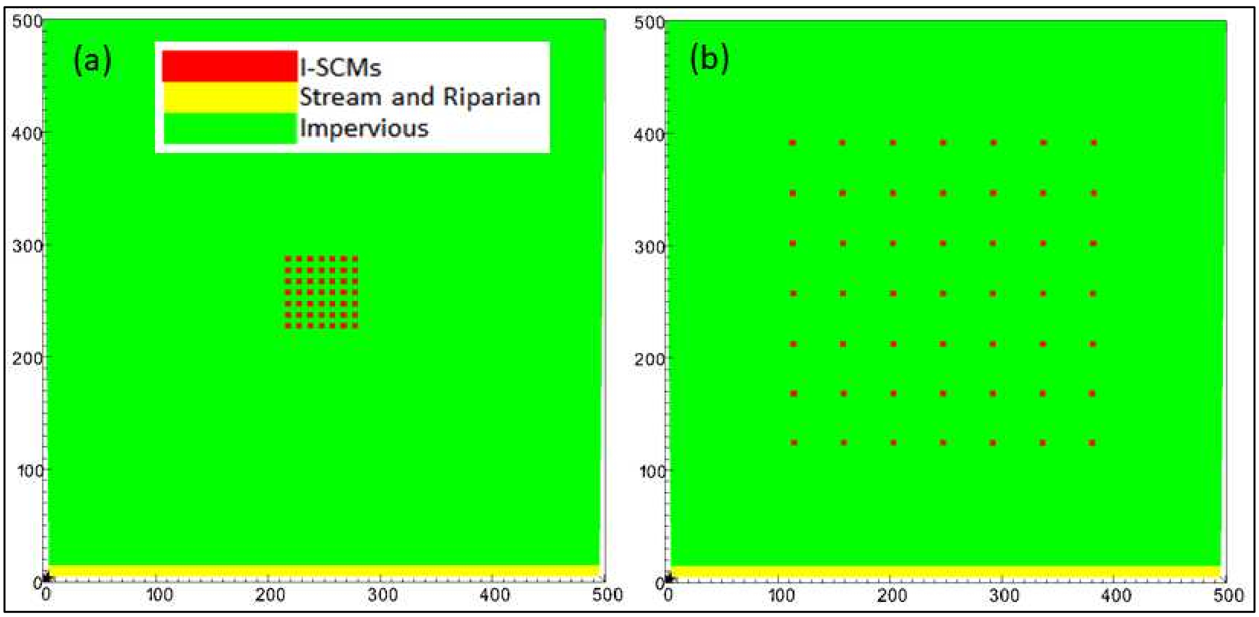

Figure 2. Top-view of model domain showing (a) clustered and (b) distributed spatial arrangements of I-SCMs. The origin (0,0) is the stream outlet of the model domain.

2.5 Spin-Up Simulations

The purpose of model spin-up is to allow modeled hydrologic conditions to reach equilibrium with average climatic forcing. Steady-state spin-up simulations were executed for each soil type and spatial arrangement of I-SCMs until daily changes in total, unsaturated zone, and saturated zone storages were all less than 0.01% of each respective storage. We ran simulations until discharge was within 1% of daily inputs because at steady-state, discharge would be equal to inputs since it was the only catchment output in spin-up simulations. The sand domain was simulated first because high conductivity soils equilibrate faster than lower conductivity soils in physically-based distributed models such as ParFlow (Seck, Welty, and Maxwell 2015). Using steady-state from the sand scenarios as initial conditions, both spatial arrangements were spun-up for the loamy sand and silt scenarios. A constant daily forcing of 0.329 m/d was applied to I-SCMs over time and was equal to the volume of annual precipitation (100 cm/yr) minus ET (40 cm/yr) over the entire impervious area. Precipitation was applied to riparian and stream cells at a rate equal to daily precipitation minus daily ET (0.16 cm/d).

2.6 Transient Simulations

After steady-state conditions were reached, we simulated transient climatic forcing that varied the pattern of inter-event durations resulting in a variety of antecedent moisture conditions. As an example of simulation time, to simulate 365 days of transient conditions on 1 computational node and 20 processors, wall clock time was 1,833 hours for the distributed sand scenario. Capturing the first 2.54 cm (1 in) of run-off is a common SCM design standard (Jefferson et al., 2017). Therefore, annual precipitation of 100 cm was applied over 40 storm events that each had rainfall of 2.5 cm over one day. All precipitation over impervious cells was introduced to I-SCMs and stormwater was applied evenly to I-SCMs such that 5 m of water was applied to each I-SCM during each 1-day event. Precipitation events were separated by interevent durations of 3, 14, and 21 days. During each of the 325 days when precipitation was not occurring, ET was set to a rate of 4.943 cm/d at I-SCM, riparian, and stream cells, totaling 0.123 cm/d or 40 cm/yr.

2.7 General Calculations

To answer our research questions we performed analyses requiring calculations of stream discharge, subsurface storage, unsaturated zone storage, and saturated zone storage, as well as hydraulic conductivities, hydraulic gradients, and Darcy flow beneath I-SCMs. Discharge, Q [m^3/d], at the catchment outlet cell was calculated using Manning's equation

$$Q_x = vA = -\frac{\sqrt{s_{o,x}}}{n} * \Psi_s^{\frac{2}{3}} * \Psi_s * \Delta y = -\frac{\sqrt{s_{o,x}}}{n} * \Psi_s^{\frac{5}{3}} * \Delta y \qquad (1)$$

where,

Q_x = discharge in x-direction out of domain [m^3/d]

v = flow velocity [m/D] = $-\frac{\sqrt{s_{o,x}}}{n} * \Psi_s^{\frac{2}{3}}$

A = cross-sectional area [m^2] = $\Psi_s * \Delta y$

$s_{0,x}$ = bed slope in x-direction [-]

n = Manning's roughness coefficient [d/m$^{1/3}$]

Ψ_s = surface ponding depth = pressure-head at outlet cell node [m]

Δy = grid-cell width in y-direction.

Subsurface storage, $V_{subsurf}$, included compressed and uncompressed storage terms and was calculated as

$$V_{subsurf} = \sum_{\Omega}[S(\psi) * S_s * \psi * \Delta x * \Delta y * \Delta z + S(\psi) * \phi * \Delta x * \Delta y * \Delta z] \qquad (2)$$

where,

Ω = all active cells in the domain

$S(\psi)$ = saturation as a function of pressure-head [-]

S_s = specific storage [1/m]

ψ = pressure-head [m]

ϕ = porosity

Δx = grid-cell width in x-direction

Δz = grid-cell width in z-direction.

Saturated zone storage was calculated by applying equation 2 to grid cells with a pressure-head greater than or equal to 0 m, and unsaturated zone storage was calculated by applying Equation (2) to grid cells with a pressure-head less than 0 m.

To investigate subsurface flow beneath I-SCMs, we computed hydraulic conductivities, hydraulic gradients, and Darcy flow between cells beneath I-SCMs and neighboring cells. Weighted hydraulic conductivities were calculated as the harmonic mean of the hydraulic conductivity in the cell of interest and neighboring cell of interest. Hydraulic gradient was calculated as the difference in hydraulic head between the cell of interest and neighboring cell of interest. Gradients were defined such that a negative gradient is away from an I-SCM. Darcy flow between cells was then calculated as,

$$q_x = -K_s * k_r(\psi) * \frac{\Delta(\psi+z)}{\Delta l} \tag{3}$$

where,

$$q_x = Darcy\ flow\ between\ cells\ in\ x - direction\ \left[\frac{m}{d}\right]$$

$$k_r(\psi) = relative\ hydraulic\ conductivity\ [-]$$

$$K_s * k_r(\psi) = hydraulic\ conductivity\ [m/d]$$

$$\Delta l = distance\ between\ cell\ centers\ [m]$$

$$\frac{\Delta(\psi+z)}{\Delta l} = hydraulic\ gradient\ [\frac{m}{m}].$$

2.8 Analyses

For both steady-state and transient simulations, mass balances with Equations (1) – (3) were calculated. For transient simulations, to identify differences in subsurface drivers of flow between scenarios, we analyzed the 2.5 m under I-SCMs for hydraulic conductivity and hydraulic gradient. We then looked at ratios of lateral flow to vertical flow on a cell-by-cell basis within the control volume defined by the horizontal size of grid cells (5 m x 5 m) and the 2.5 m depth beneath each I-SCM. For lateral flows, vertical cell height was normalized by the smallest vertical discretization of 0.5 m. We did this so flow at larger cells would be counted more than flow at smaller cells since the volumetric flow at the same flux would be greater for larger cells (i.e., 1 m vertical cell counted as two data points while 0.5 m vertical cell counted as one). We calculated Darcy flow for the four lateral faces of each cell and the ratio of lateral flow to vertical flow was calculated for each cell face (i.e., four ratios of lateral to vertical flow for each 0.5 m vertical span).

Results were then compared between spatial arrangements and soil types addressing questions 1 and 3. We compared plant available water in I-SCM cells and all cells within the layer just beneath the impervious layer, which we refer to as the root zone. Plant available water was calculated for each day by applying Equation (2) to those cells where pressure head was greater than wilting point (-153 m).

Catchment discharge was compared between spatial arrangements and soil types. We compared discharge on the day after a precipitation event to the discharge the day before the following precipitation event and determined the timing of maximum baseflow following each precipitation event to characterize baseflow recession behavior. Then, to investigate effects of antecedent precipitation, defined here as precipitation depth in previous 15 days, we binned rate of change and timing of maximum discharge with depth of precipitation in the previous 15 days. To quantify and compare effects of I-SCM spatial arrangement on groundwater mounding we compared depth to water table (DTWT) on the wettest day and driest day of the simulation based on precipitation received in the previous 15 days. Precipitation within the previous 15 days was calculated for each day of the transient simulations (after day 15). Several days resulted in the same antecedent precipitation, so we defined the wettest day as the day farthest into the simulated year with the most antecedent precipitation that was also the day after a precipitation event. The driest day was defined as the day farthest into the simulated year with the least antecedent precipitation that was also the day before a precipitation event.

Chapter 3: Results

3.1 Steady-State Mass Balance

First, we examined the effects of I-SCM spatial arrangement and soil type on steady-state mass balance components of unsaturated storage, saturated storage, total subsurface storage, and surface storage (Table 2). Discharge was not considered since P-ET forcings were constant between scenarios and so, at steady-state, discharges were the same.

Unsaturated storage was of similar magnitude for all soils and I-SCM spatial arrangements (Table 2), but differences in unsaturated storage between I-SCM spatial arrangements were greater in silt than in loamy sand and were greater in loamy sand than in sand (Table 2). In silt, clustered I-SCMs led to nearly 67,000 m^3 or 31% more unsaturated storage than distributed I-SCMs. In contrast, in the other two soils, distributed I-SCMs produced more unsaturated storage than clustered I-SCMs (18,881 m^3 or 8.4% in loamy sand and 9,471 m^3 or 4.2% in sand). Focusing just on clustered I-SCMs, silt had the largest unsaturated storage, followed by sand. Under distributed I-SCMs, silt soil had the least unsaturated storage, followed by loamy sand.

Differences in saturated and total subsurface storage were larger between soils than between I-SCM spatial arrangements. Total subsurface storage was the least different measure of storage between I-SCM arrangements. Silt had more total subsurface storage than loamy sand (~1.1 million m^3 on average or 41% different) or sand (1.6 million m^3 on average or 70% different), in both the clustered and distributed scenarios. Loamy sand had more subsurface storage than sand (about 0.57 million m^3 or 28% more) in both I-SCM arrangements. The percent difference patterns among soils for saturated storage were similar to those in total storage differences, but the magnitudes were larger. Under distributed I-SCMs, silt resulted in 44% more saturated storage than loamy sand 69% more than sand. Under clustered I-SCMs silt produced 38% more saturated storage than loamy sand and 73% more than sand. Within soils saturated storage was greater under distributed I-SCMs where unsaturated storage was less under distributed I-SCMs, and the same was true for clustered I-SCMs. In silt soil distributed I-SCMs resulted in 127,708 m^3 more saturated storage than clustered I-SCMs. In loamy sand and sand soils distributed I-SCMs produced less saturated storage than clustered I-SCMs (15,731 m^3 less in loamy sand and 3,280 m^3 less in sand).

Surface storage was identical between I-SCM arrangements in sand and loamy sand and nearly identical between those two soils, but silt soil produced very contrasting results. Severe groundwater mounding was observed in the silt soil at steady-state. While surface ponding occurred over a greater area under distributed I-SCMs, the total volume of surface ponding was 131% (6,529 m^3) greater under clustered I-SCMs. Due to this groundwater mounding and surface ponding at steady-state, silt soil scenarios were not included in transient results.

Table 2. Mass balance resulting from steady-state spin-up simulations. The percent difference in storage between distributed and clustered arrangements for each soil type was calculated as $|V_2 - V_1|/(\frac{V_2+V_1}{2})$, V_2=Value 2 and V_1=Value 1.

Soil	Sand		Loamy Sand		Silt	
Arrangement	Clustered	Distributed	Clustered	Distributed	Clustered	Distributed
Unsaturated Storage [m3]	221,839	231,310	216,109	234,990	249,695	182,926
Difference [m]	0.04		0.08		0.27	
% Difference	4.2%		8.4%		30.9%	
Saturated Storage [m3]	1,500,666	1,497,386	2,074,876	2,059,145	3,079,016	3,206,724
Difference [m]	0.01		0.06		0.51	
% Difference	0.2%		0.8%		4.1%	
Subsurface Storage [m3]	1,722,505	1,728,695	2,290,984	2,294,135	3,328,710	3,389,651
Difference [m]	0.02		0.01		0.24	
% Difference	0.4%		0.1%		1.8%	
Surface Storage [m3]	24	24	25	25	8,231	1,702
Difference [m]	0		0		0.03	
% Difference	0.0%		0.0%		131.5%	

3.2 Transient Mass Balance

Next, we examined the effects of I-SCM spatial arrangement and soil type on transient catchment mass balances. Similar to steady-state results, the magnitude of differences in unsaturated storage between soils was similar to that between I-SCM spatial arrangements within soils (Figure 3a). There was more unsaturated storage in the distributed scenarios compared to clustered scenarios throughout transient simulations. In loamy sand, the distributed scenario had between 16,942 m^3 and 24,611 m^3

(mean of 20,641 m^3) more unsaturated storage than the clustered scenario (Figure 3b). In sand, the distributed arrangement had more unsaturated storage (mean of 10,250 m^3) than clustered, and the difference varied from 6,953 m^3 to 13,168 m^3. Unsaturated storage showed more temporal variability in loamy sand compared to sand; increasing between precipitation events as saturated storage drained. In general, the partitioning of storage between unsaturated and saturated zones was more dynamic than total subsurface storage. Unsaturated storage had an overall decreasing trend through time, with this trend being stronger in the loamy sand. Although there was an overall decrease, the differences between spatial arrangements in each soil remained similar throughout the simulations.

For saturated storage, the differences between spatial arrangements within soils were small compared to those between soils (Figure 3c). Loamy sand had more saturated storage than sand (589,296 m^3 more under clustered I-SCMs and 576,812 m^3 more under distributed I-SCMs), and these differences were one to two orders of magnitude larger than differences between I-SCM spatial arrangements. Saturated storage was consistently greater in the clustered I-SCM scenario compared to the distributed I-SCM scenario. Differences in saturated storage between I-SCM arrangements remained relatively constant through time. In the loamy sand differences oscillated about the mean of 16,738 m^3 ranging from 9,806 m^3 to 20,525 m^3 more under clustered I-SCMs (Figure 3d). In the sand, differences oscillated about the mean of 4,255 m^3 ranging from 831 m^3 to 7,091 m^3 more under clustered I-SCMs. These differences in saturated storage between I-SCM arrangements (where clustered arrangements were larger) were less than differences in unsaturated storage (where distributed arrangements were larger), resulting in consistently greater total subsurface storage under distributed I-SCMs. Saturated storage had an increasing trend through time for all scenarios and this trend was larger in loamy sand.

Similar to saturated storage, total subsurface storage resulted in differences between spatial arrangements within soils being small compared to those between soils (Figure 3e). Distributed I-SCMs had greater total subsurface storage than the clustered scenarios (3,902 m^3 in loamy sand and 5,995 m^3 in sand), but these differences were two orders of magnitude smaller than storage differences between soils. Loamy sand had more total subsurface storage than sand on average (577,252 m^3 more under clustered I-

SCMs and 575,160 m^3 more under distributed I-SCMs). Total subsurface storage also showed an increasing trend through time, but the change was smaller than that for saturated storage. Loamy sand subsurface storage increased more through time than sand. Differences in subsurface storage between spatial arrangements remained similar through time in sand and loamy sand with small fluctuations about the mean (Figure 3f).

Differences in discharge magnitude and behavior were larger between soil types than between I-SCM arrangements (Figure 3g and 3h). The sand scenarios generally had higher discharge than the loamy sand scenarios (69.4 m^3/d more under clustered I-SCMs and 65.3 m^3/d more under distributed I-SCMs on average). For loamy sand, discharge was larger throughout the transient simulations under distributed I-SCMs with the exception of two dry periods, once during the initial recession from steady-state conditions and once leading up to the 36th precipitation event occurring on day 333. The sand scenario experienced greater variability in discharge compared to loamy sand, but differences between spatial arrangements were smaller on average than in loamy sand. Discharge in all scenarios showed an increasing trend through time with sand discharges increasing a greater magnitude. Differences in discharge response to precipitation were quite different between soils and results presented below (Figure 4 and 5) further highlight this fact. In general, distributed I-SCMs produced greater baseflow during wet periods while clustered I-SCMs produced greater baseflow during dry periods (Figure 3h). This relationship was more pronounced in the sand catchment compared to the loamy sand catchment.

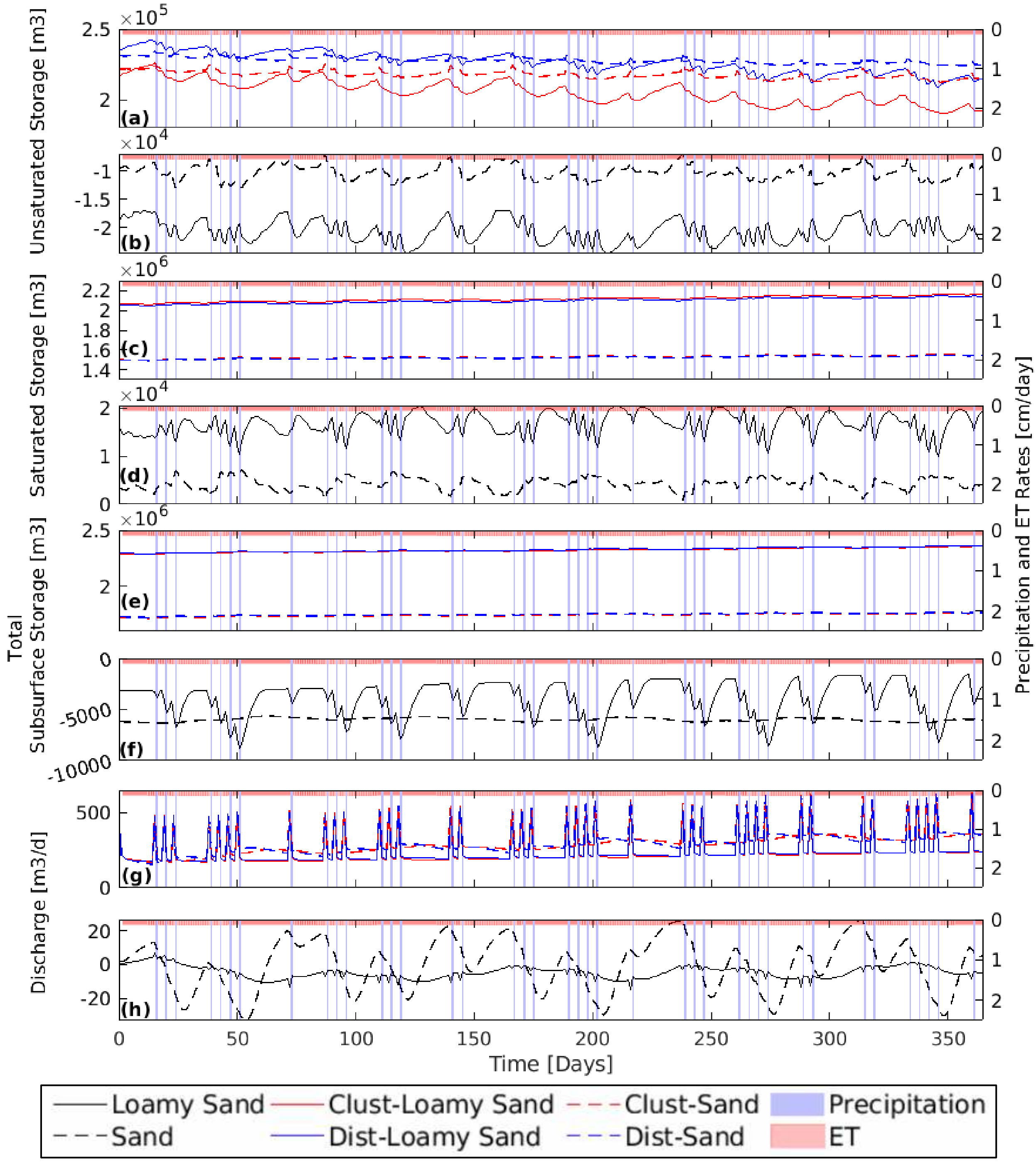

Figure 3. Catchment mass balances: (a) unsaturated storage, (b) differences in unsaturated storage between arrangements (clustered minus distributed), (c) saturated storage, (d) differences in saturated storage between arrangements, (e) total subsurface storage, (f) differences in total subsurface storage between arrangements, (g) stream discharge (h) differences in discharge between arrangements. Precipitation and ET hyetographs are shown behind the mass balance components in each panel. Note that the y-axes for (a), (b), (c), and (e) do not start at 0. In panels showing differences positive numbers (+) represent greater clustered values and negative numbers (-) represent greater distributed values, red lines represent differences in loamy sand and blue lines represent differences in sand.

3.3 Discharge Recession

Recession rate, or the rate of change of discharge during inter-event periods, became closer to zero with greater precipitation occurring in the previous fifteen days (Figure 4). For loamy sand, the recession rate was similar between spatial arrangements (Figure 4a and 4b). In sand, recession rate showed a stronger relationship to antecedent precipitation compared to loamy sand (Figures 4c and 4d). In the clustered sand scenario (Figure 4c), this relationship was strongest and increases in discharge during recession periods were occasionally observed.

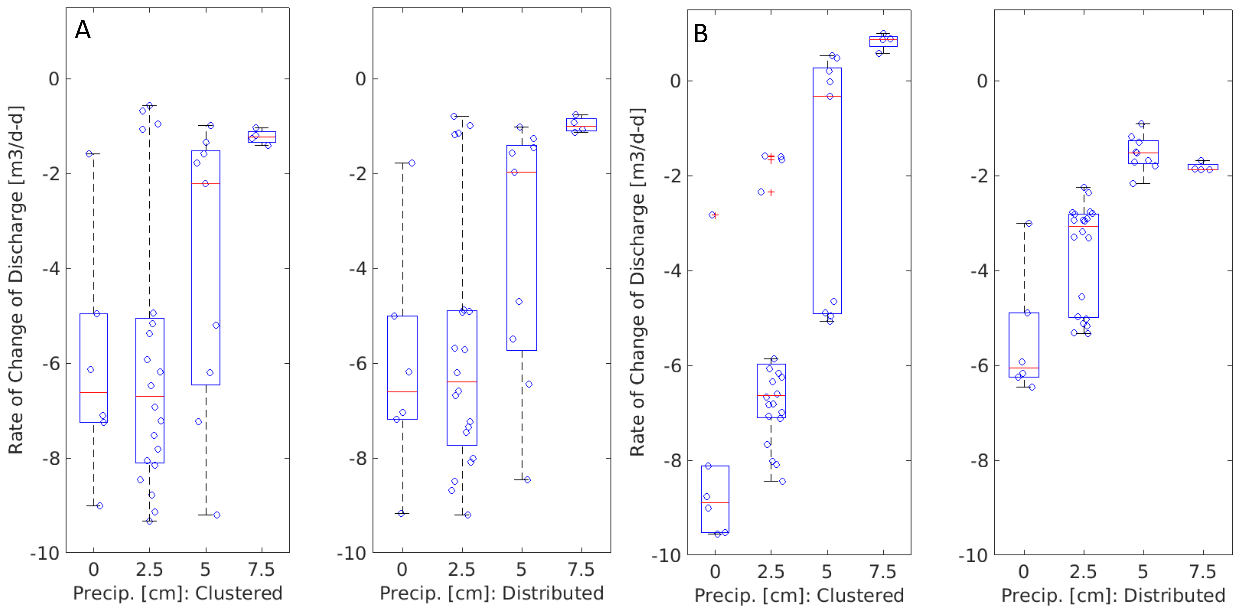

Figure 4. Loamy sand rate of change of discharge during inter-event periods (y-axis) vs. precipitation depth in the previous 15 days (x-axis) for (a) clustered and (b) distributed. Sand rate of change of discharge during inter-event periods (y-axis) vs. precipitation depth in the previous 15 days (x-axis) for (c) clustered and (d) distributed.

For loamy sand, the day following a precipitation event was always the day with the largest magnitude baseflow between events (Figures 5a and 5b). Similar to what was observed with recession rates (Figure 4c and 4d), spatial arrangement magnified the effects of antecedent precipitation on days until maximum discharge in the sand (Figures 5c and 5d), and especially in the clustered sand scenario (Figure 5c). In the clustered sand scenario 9 of the 39 inter-event durations had maximum baseflow 8 to 14 days after the precipitation event. Eight of those 9 inter-event durations were following 5 cm or 7.5 cm of precipitation in the previous fifteen days. When there was 7.5 cm of antecedent precipitation, the maximum baseflow never occurred before 12 days after a precipitation event. In the distributed sand scenario, the largest period of time until maximum baseflow was five days (Figure 5d).

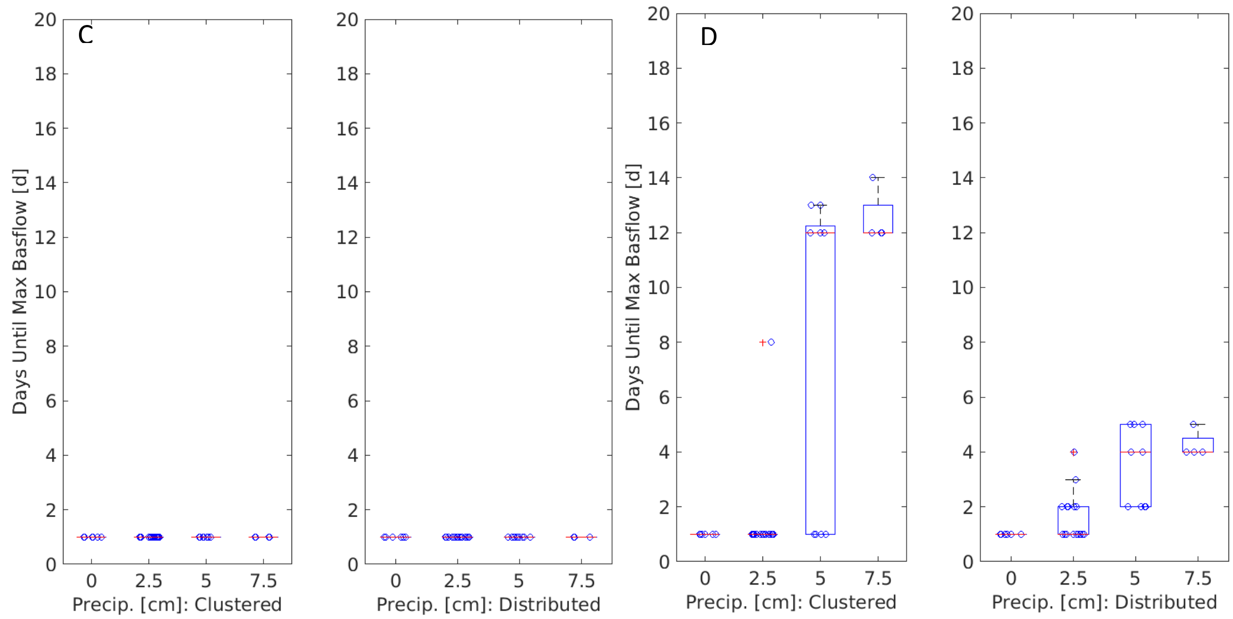

Figure 5. (a) Loamy sand, days after precipitation event until maximum baseflow is observed (y-axis) vs. precipitation depth in previous 15 days (x-axis). (b) Sand, days after precipitation event until maximum baseflow is observed (y-axis) vs. precipitation depth in previous 15 days (x-axis).

3.4 Depth to Water Table

While Figures 3-5 present spatially-integrated temporally-variable conditions, we also examined spatial variability of depth to water table and plant available water within the model domain. Loamy sand (Figures 6a-d) had an overall shallower depth to water than sand (Figures 6e-h) (6.64 m vs. 12.16 m on average). The shallowest depth to water table was on the wet day with clustered I-SCMs and loamy sand soil (Figure 6b), a case in which there was also mounding (shown in white). In the sand scenario both spatial arrangements were able to infiltrate all water without mounding, but in the loamy sand scenario the clustered arrangement resulted in periodic mounding. Infiltrated water affected water table elevation over a greater area in the loamy sand scenario (Figure 6a,b,c, and d vs 6e,f,g, and h).

In general, between I-SCM arrangements distributed I-SCMs maintained larger average depth to water table (DTWT) over the domain (Figure 6) and sand resulted in average DTWTs nearly double that of loamy sand. Averaging DTWTs under I-SCMs showed that distributed I-SCMs produced greater

DTWT directly under I-SCMs in all scenarios except wet loamy sand, where all I-SCMs saturated under both I-SCM arrangements (Figure 6b and 6d).

Using domain averaged DTWT from the wet and dry day to estimate aquifer thickness, aquifer diffusivities were determined to be 65.8 m^2/d under clustered I-SCMs in loamy sand, 65.4 m^2/d under distributed I-SCMs in loamy sand, 316.5 m^2/d and 315.7 m^2/d under clustered and distributed I-SCMs in sand, respectively.

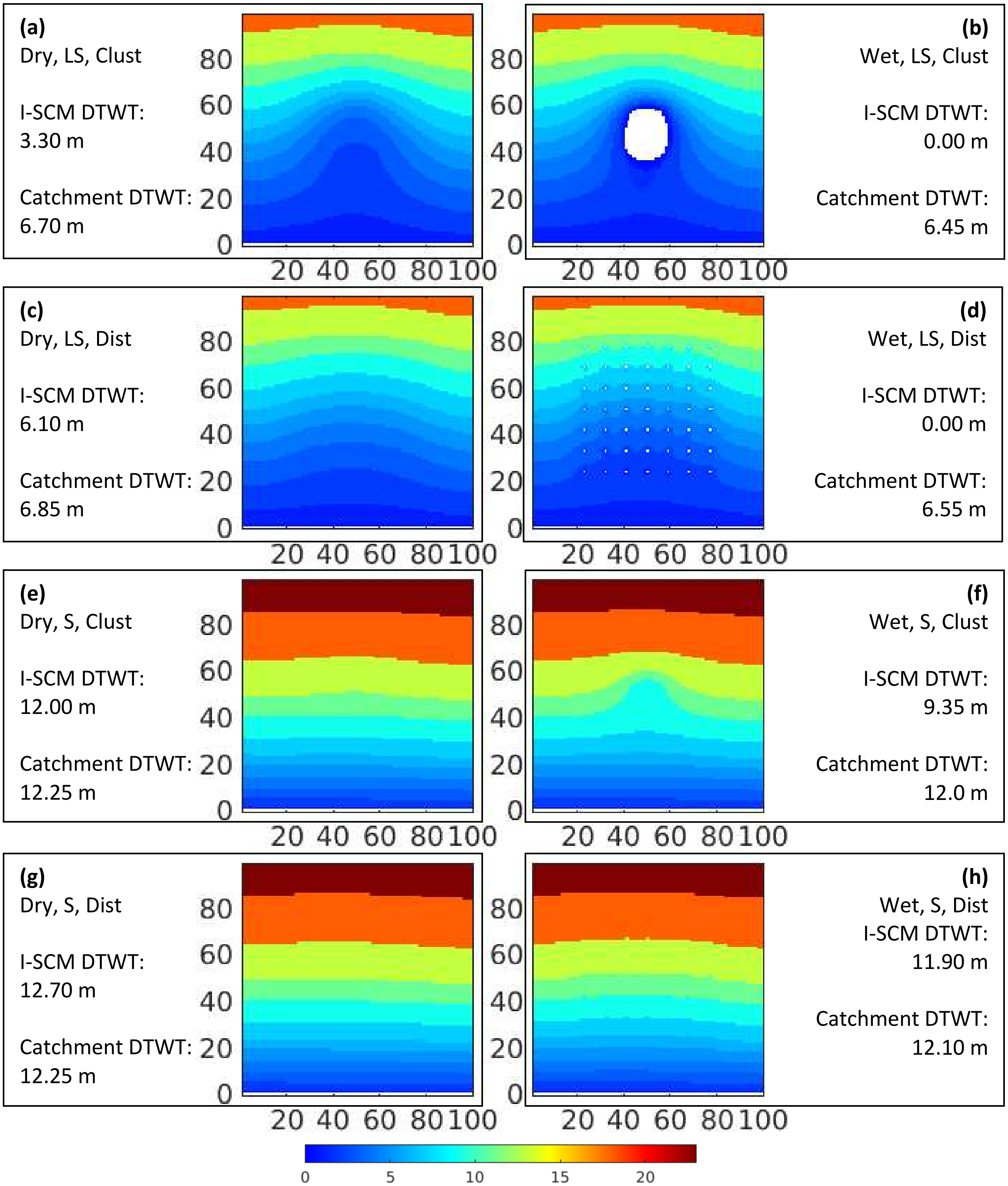

Figure 6: Depth to water table (a) Dry, loamy sand, clustered (b) Wet, loamy sand, clustered (c) Dry, loamy sand, distributed (d) Wet, loamy sand, distributed (e) Dry, sand, clustered (f) Wet, sand, clustered (g) Dry, sand, distributed (h) Wet, sand, distributed. White shows locations where groundwater elevation has reached or exceeded surface elevation. Catchment outlet is at origin (bottom left corner). Text shows scenario: Loamy Sand [LS] or Sand [S], and Clustered [Clust] or Distributed [Dist]; Average DTWT directly under I-SCMs [I-SCM DTWT], and catchment average DTWT [Catchment DTWT].

To complement analysis of depth to water table, we compared plant available water between I-SCM spatial arrangements (Figure 7). As expected, during the wet day, plant available water was greater in the distributed scenario at the distributed I-SCM locations (green in Figure 7) and was greater at the clustered I-SCM locations in the clustered arrangement (blue). On the dry day in the loamy sand, the opposite was observed, where the clustered scenario had more plant available water at the location of distributed I-SCMs and vice versa. A more muted effect was seen on the dry day in sand where the differences between the arrangements became negligible at several I-SCM locations. This occurred during inter-event durations due to ET removing moisture at different locations (at I-SCMs) for each I-SCM spatial arrangement (Figure 7a and 7c). Loamy sand had double the plant available water across the root zone compared to sand for each scenario. In the loamy sand clustered I-SCMs resulted in 0.41% more plant available water than distributed I-SCMs on the dry day and 3.8% more on the wet day. Sand resulted in 1.6% and 2.2% less plant available water under clustered I-SCMs compared to distributed I-SCMs on the dry and wet days, respectively.

While overall volumes of plant available water in the root zone were similar between I-SCM arrangements, different areas of the domain were wetted depending on spatial arrangement, especially for loamy sand (Figure 7a and 7b).

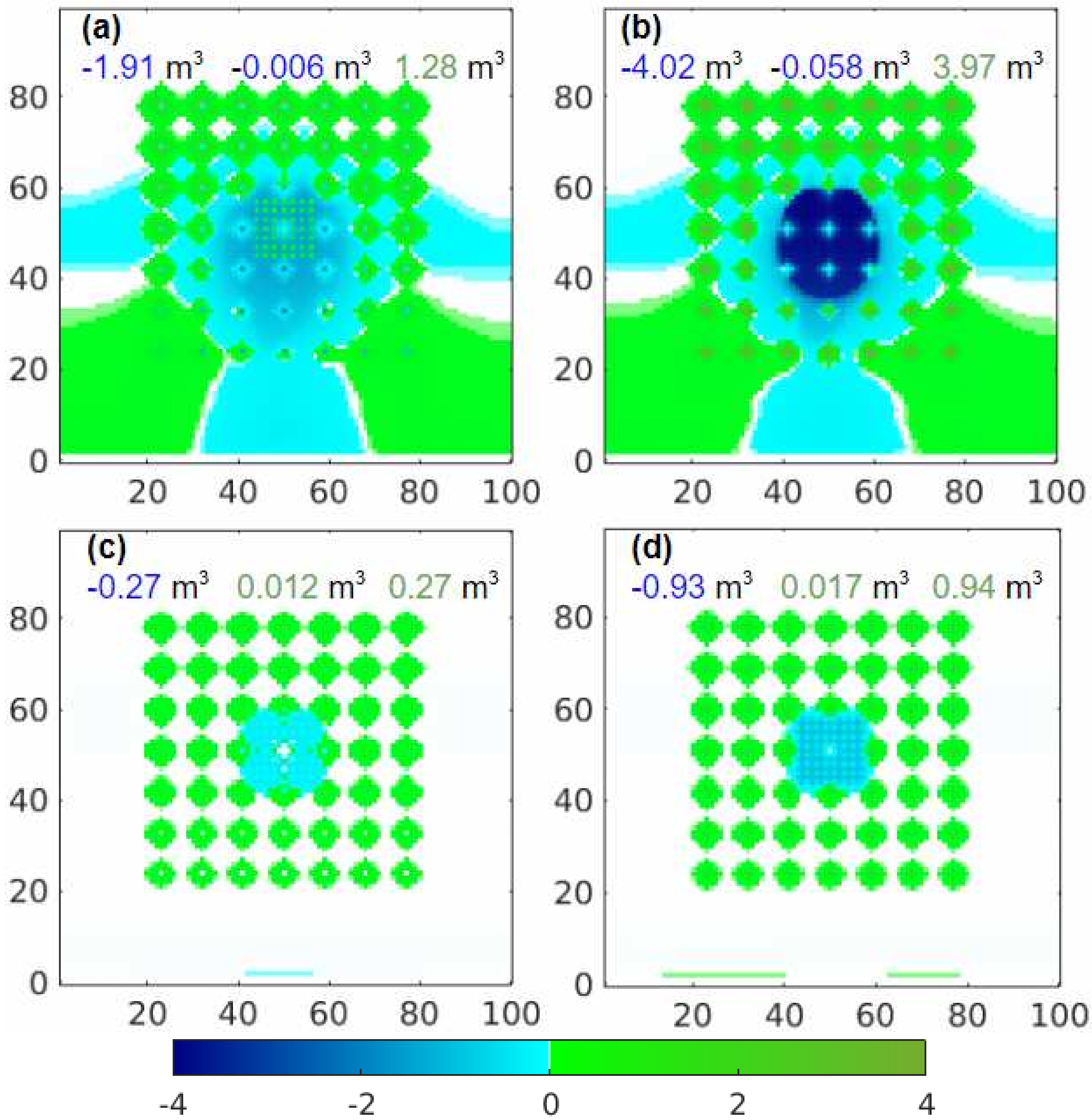

Figure 7: Differences for distributed – clustered arrangements in plant available water [m^3] per each cell [12.5 m^3] in the root zone (between 0.5 m and 1 m below the surface layer just beneath impervious layer) for (a) Loamy sand dry day (b) Loamy sand wet day (c) Sand dry day (d) Sand wet day. Negative values (blue) represent greater plant available water for the clustered I-SCM arrangement and positive values (green) represent greater plant available water for distributed I-SCM. Catchment outlet is at origin (bottom left corner). Text values of plant available water differences from left to right: magnitude of minimum (clustered exceeds distributed by largest amount), mean (color of text shows which arrangement is greater), and maximum (distributed exceeds clustered by largest amount) of all cells.

3.5 Subsurface flow drivers

To examine the drivers of flow beneath I-SCMs, we compared unsaturated hydraulic conductivity, lateral hydraulic gradients, and the product of the two (Darcy Flow) (Figure 8). In both sand and loamy sand, a clustered arrangement resulted in larger lateral hydraulic conductivities beneath I-SCMs (Figure 8a), as soil moisture was higher beneath clustered I-SCMs (Figure 7). Hydraulic gradients reversed between towards I-SCMs during long, dry periods and away from I-SCMs during rainfall (Figure 8b). During wet periods, which were of particular interest, distributed I-SCMs resulted in greater lateral hydraulic gradients away from I-SCMs but smaller hydraulic conductivities. Spatial arrangement affected subsurface lateral flow drivers of hydraulic conductivity and hydraulic gradient more strongly in the loamy sand compared to sand (Figure 8a and 8b). Resulting lateral Darcy flows were greater for the clustered spatial arrangement during all times (Figure 8c). Although there were hydraulic gradients toward the I-SCMs during inter-event periods, these correspond to low soil moisture when hydraulic conductivity is low, resulting in small Darcy flow (Figure Fc). We presented medians of subsurface flow drivers as these captured the overall patterns of interest.

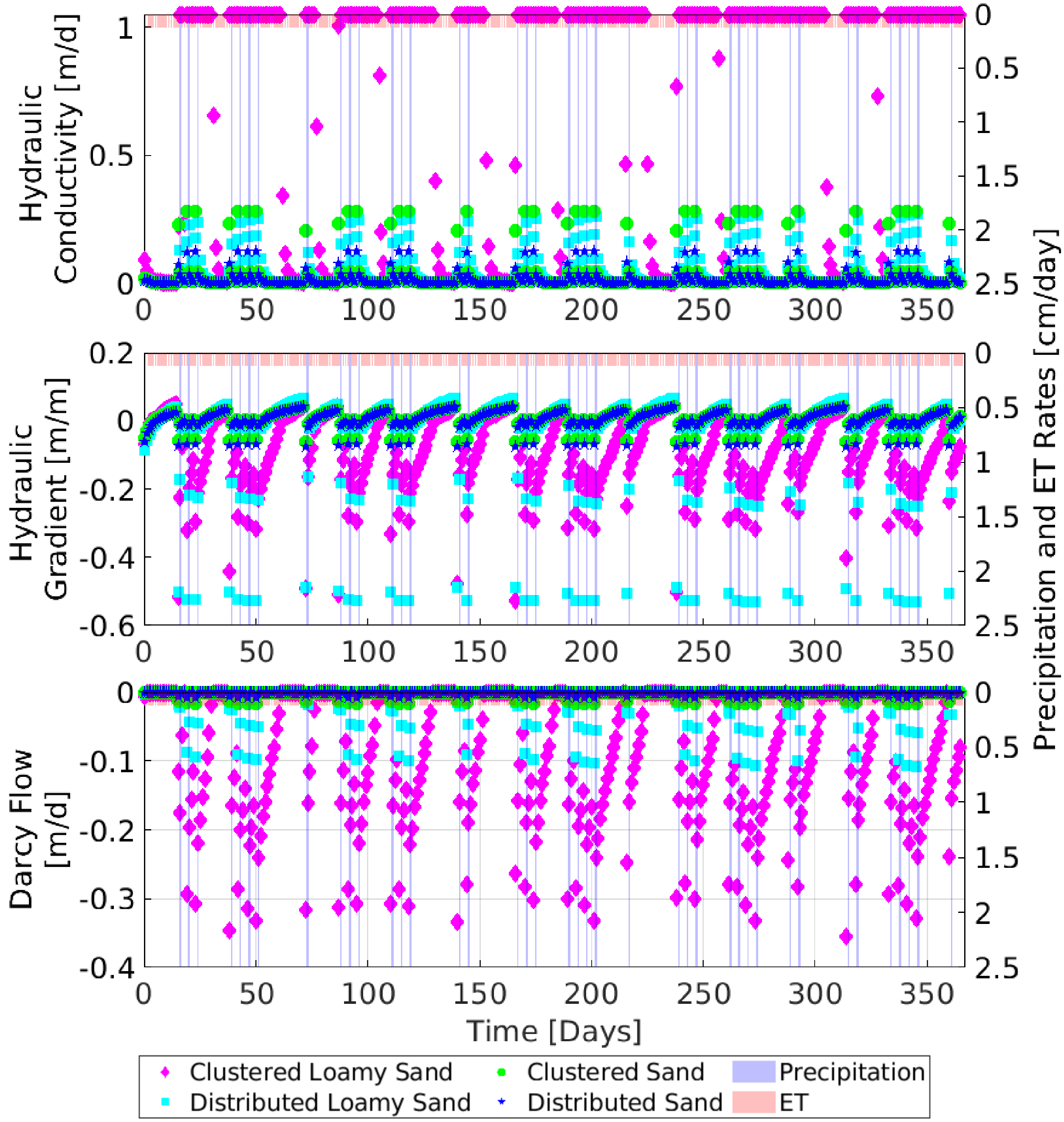

Figure 8: Medians of lateral flow drivers (a) hydraulic conductivity, (b) hydraulic gradient, and (c) Darcy flow approximations within 2.5 m below I-SCMs. Negative values (-) for hydraulic gradient and Darcy flow represent gradients and flows away from I-SCMs and positive values (+) represent gradients and flows towards I-SCMs.

Similar to drivers of lateral flow, drivers of vertical flow were more sensitive to I-SCM spatial arrangement in the loamy sand soil than the sand soil. In sand, hydraulic conductivities never reached saturated hydraulic conductivity and were similar between I-SCM arrangements, although clustered I-

SCMs produced slightly larger conductivities on days of precipitation (Figure 9a). Loamy sand vertical hydraulic conductivities reached saturated hydraulic conductivity (1.05 m/d) under both I-SCM arrangements on days with precipitation, although saturated conditions lasted longer for clustered I-SCMs compared to distributed. Sand hydraulic conductivities were still larger than those of loamy sand during precipitation. Vertical hydraulic gradients were consistently away from the I-SCMs (downward), although the gradients became closer to 0 during dry periods (Figure 9b). During precipitation, vertical hydraulic gradients were most strongly downward in the distributed loamy sand scenario and smallest in the clustered loamy sand scenario. Hydraulic gradients in both sand scenarios fell between the two loamy sand scenarios and tended to stay at or just below the unit downward gradient (-1 m/m). The unit gradient occurs when pressure gradients are negligible and gravity drives flow. Hydraulic head gradients with an absolute magnitude smaller than 1 (0 to -1) suggested an upward pressure head gradient and hydraulic head gradients with a larger absolute magnitude than -1 m (-1 m to –infinity) resulted from downward pressure head gradient. When we combine hydraulic conductivity and vertical gradient, the largest vertical Darcy flow was seen during days of precipitation in clustered sand and distributed sand scenarios, followed by the distributed loamy sand scenario, then the clustered loamy sand scenario (Figure 9c). The clustered loamy sand scenario is the only one that had significant vertical flow persist during days without precipitation.

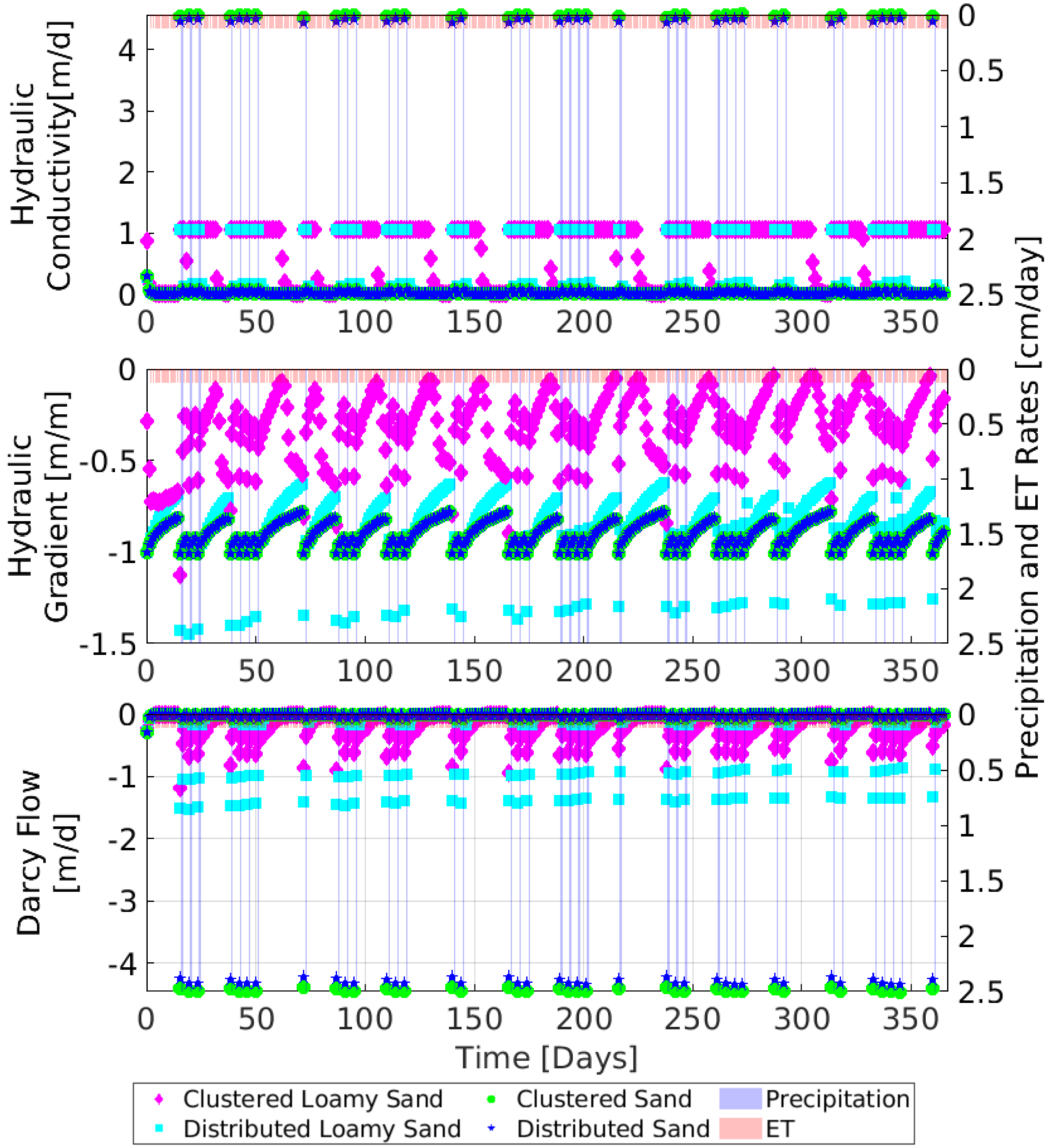

Figure 9: Medians of vertical flow drivers including hydraulic conductivity, hydraulic gradient, and Darcy flow approximations. Negative values (-) for hydraulic gradient and Darcy flow represent gradients and flows away from I-SCMs (downward) and positive values (+) represent gradients and flows towards I-SCMs (upward).

Ratios of lateral to vertical Darcy flow were less than 1 indicating vertical flow was dominant over horizontal flow (Figure 10). The ratio of lateral to vertical flow increased during wet periods as lateral flow increased with infiltration, and became close to 0 or negative during dry periods. The only days resulting in median ratios greater than 0.5 occurred after four precipitation events within a thirteen day time period (10 cm/13 days), and that was only observed in the clustered loamy sand scenario. Loamy sand also resulted in the most negative ratios occurring during inter-event periods and resulting from small vertical gradients away from I-SCMs and large (relative to other scenarios) lateral gradients towards I-SCMs. The other three scenarios showed very similar ratios and were much less variable through time.

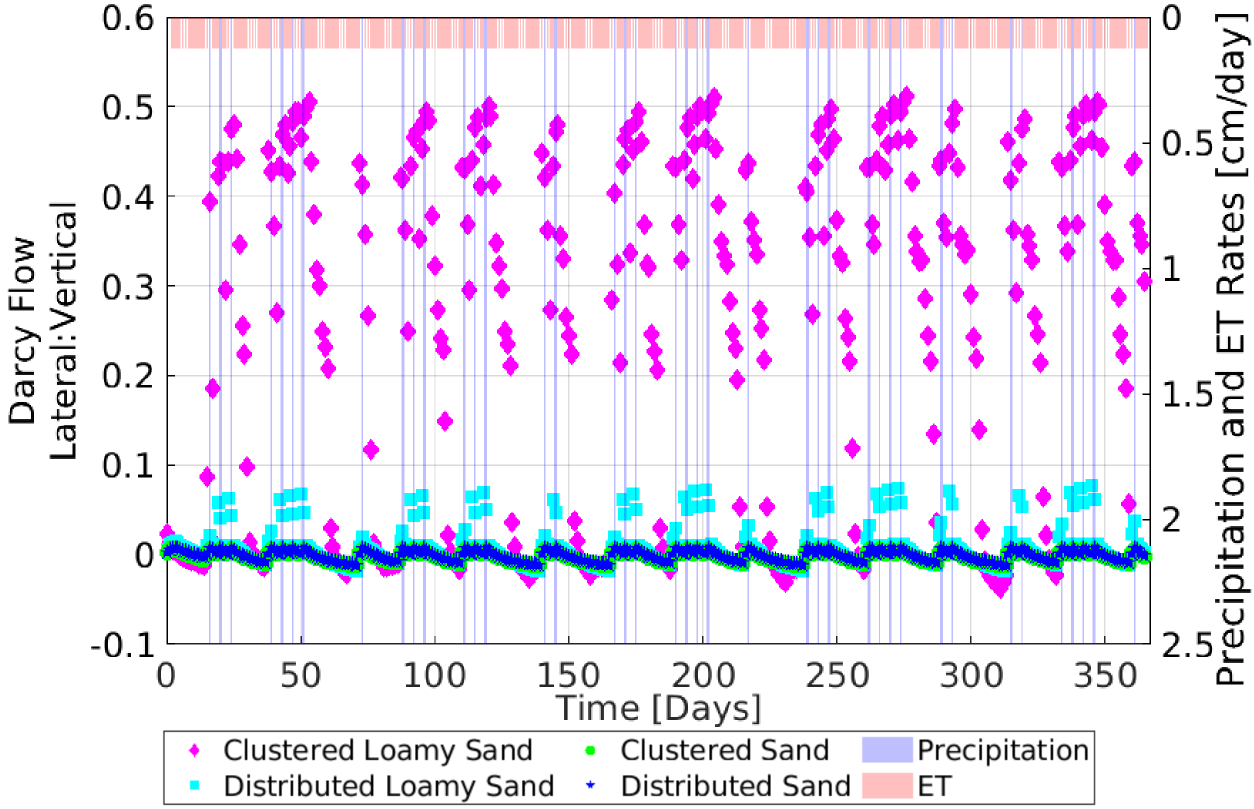

Figure 10: Median ratio of lateral to vertical Darcy flow. Negative values (-) result when lateral flow and vertical flow are in opposite directions (e.g., lateral flow towards I-SCMs and vertical flow away from I-SCMs) and positive values which are most prevalent show scenarios where both flows are either towards or away from I-SCMs.

Chapter 4: Discussion

4.1 Dynamic equilibrium of transient simulations

Unsaturated, saturated, and total subsurface storage had trends over the course of the transient simulations (Figure 3). Unsaturated storage decreased over time, with a larger decrease in loamy sand (~200,000 m^3) than sand (~10,000 m^3). Saturated storage increased over time by the same order of magnitude that unsaturated storage decreased, but as a percent change, the decreases in saturated storage were smaller since the volume of saturated storage was an order of magnitude larger than that of unsaturated storage. Total subsurface storage also increased over time, showing that saturated storage increased a greater magnitude through transient simulations than the magnitude unsaturated storage decreased. The transient simulation started with 14 days of ET. During this time, discharge dropped to 38-43% of steady-state discharge in all scenarios (Figure 3g). By the end of the simulation loamy sand discharge had reached 58% of the steady-state discharge under both I-SCM arrangements and sand had reached 87% and 85% of steady-state discharge under clustered and distributed I-SCMs, respectively.

The steady-state spin-up had the same average P-ET as the transient simulations, but for the steady-state spin-up P-ET was applied as a constant low rate of input. Although using an average climatic forcing for steady-state spin-up is a common approach, the trend seen in the transient simulation away from the steady-state initial condition indicates that the temporal pattern of P-ET affects storage and discharge magnitudes. The temporal trends observed in storage during transient simulations are due primarily to decreased discharge. As net inputs (P-ET) were consistent between spin-up and transient simulations, decreased discharge in the transient simulations led to increased total and saturated storage. As saturated storage increased, unsaturated storage decreased. We suspect discharge decreased so dramatically from steady-state to the beginning of the transient simulation because transient wetting-drying cycles produced different distributions of water table elevations and hydraulic gradients than the constant, low intensity forcings applied in spin-up. Altered hydraulic gradients near the stream in the transient simulation compared to the steady-state simulation may have driven diminished discharge observed in transient simulations.

These temporal trends limit our analysis of differences in unsaturated storage magnitude between soils. However, we are still able to analyze the two key aspects of the transient simulations important to our research questions: response to precipitation events between soils and spatial arrangements, and the difference in unsaturated storage magnitude between spatial arrangements within a soil. Both of these characteristics remained relatively consistent over time (Figure 3a and 3b). Differences in saturated storage (Figure 3d) and discharge (Figure 3f) between I-SCM arrangements also remained consistent throughout transient simulations. Differences in total subsurface storage between I-SCM arrangements remained consistent in sand while loamy sand saw a small decreasing trend in differences (towards 0) (Figure 3f). Therefore, we were able to use the transient simulations to analyze the differences between spatial arrangements and response to precipitation between all scenarios.

4.2 Subsurface storage and baseflow

Distributed I-SCMs always resulted in more unsaturated storage than clustered I-SCMs (Figure 3a), which is also reflected in greater average DTWTs under distributed I-SCMs (Figure 6). In general, unsaturated storage decreased in response to precipitation, as unsaturated cells became saturated, and increased during inter-event periods, as saturated cells became unsaturated. Since clustered I-SCMs led to more unsaturated cells becoming saturated during precipitation than distributed I-SCMs (compare Figures 6b and 6d), unsaturated storage decreased more during precipitation events and increased more during dry periods for clustered as compared to distributed I-SCMs (Figure 4). During precipitation, the distributed scenario had more rapid and short-lasting (1 day) decreases in unsaturated storage with rapid and short-lasting increases during short (3 day) interevent durations where clustered I-SCMs resulted in smoother decreases during precipitation events, particularly evident for the loamy sand (Figure 3a). This suggests distributed I-SCMs recover infiltration capacity faster than clustered I-SCMs as saturated cells quickly dewater under distributed I-SCMs compared to clustered I-SCMs.

I-SCM spatial arrangement affected unsaturated storage as much as soil type. Steady-state results (Table 2) suggested I-SCM arrangement actually had stronger effects on unsaturated storage than soil type, but during transient simulations, differences in unsaturated storage became larger between soils (Figure 3a). Unsaturated storages could be similar between soils due to a trade-off between greater depths to water table in sand providing more unsaturated area, loamy sand holding more water than sand at a given pressure-head, and shallower DTWTs in loamy sand increasing pressures within the unsaturated zone. Throughout transient simulations, loamy sand resulted in larger episodic (i.e., in response to precipitation) changes in unsaturated storage than did sand. This reflects fewer cells becoming saturated in sand and more becoming saturated in loamy sand during precipitation, which fits with the mounding observed in loamy sand (Figure 6).

Clustered I-SCMs had greater saturated storage than distributed I-SCMs (Figure 3c), which mirrors the differences in spatial arrangement observed in unsaturated storage (Figure 3a). Although spatial arrangement of I-SCMs had a consistent effect on saturated storage, the largest saturated storage differences observed between scenarios were between soil types. Spatial arrangement had a stronger effect on saturated storage in loamy sand than sand, similar to unsaturated storage (Figure 3d). We attribute this to distributed I-SCMs having infiltration sites at higher elevations than clustered I-SCMs. This meant there was a larger difference in unsaturated depth under I-SCMs between arrangements during dry days in loamy sand (Figure 6). Having I-SCMs at higher elevation, resulting in greater DTWTs, also generates greater downward hydraulic gradients during precipitation (Figure 9b light blue squares) driving infiltrated water into the deeper unsaturated zone only present at higher elevation I-SCMs. This is only possible because the surface slope towards the stream was greater than that of the water table surface slope (hydraulic grade line). In sand there was even greater DTWTs, but the soil was so permeable vertical hydraulic gradients remained small as water moved before significant gradients could form at the precipitation rates applied resulting in median vertical hydraulic gradients in the unsaturated zone never exceeding the gravity driven unit hydraulic gradient (1 m/m downward) (Figure 9b light blue dark blue stars and green circles). Under clustered I-SCMs in the loamy sand hydraulic gradient rarely exceeded the unit hydraulic gradient and gradients tended to stay smaller than other scenarios (Figure 9b pink diamonds) as DTWTs under I-SCMs were relatively shallow (Figure 6a and 6b).

As expected, during spin-up, lower permeability soils had more saturated storage (Table 2). In silt at steady-state, there was severe groundwater mounding throughout much of the domain (Table 2). With distributed I-SCMs, 12 of 49 I-SCMs remained unsaturated with distributed I-SCMs and in the clustered scenario, all I-SCMs saturated. In silt, the clustered I-SCMs had greater surface storage than distributed I-SCMs (Table 2), but also left more unsaturated area up elevation gradient, whereas distributed I-SCMs infiltrated water to that area leading to greater saturated storage in the silt steady-state scenario.

Differences in total storage between I-SCM arrangements were small compared to unsaturated or saturated storage in terms of both magnitude, and percent difference. Similar to other storages though, differences between I-SCM arrangements were more dynamic in loamy sand compared to sand. While total storage did change over time, there was more dynamism in the interaction between saturated and unsaturated storages than in total storage.

We expected distributed I-SCMs to produce more plant available water throughout the root zone because of the deeper water tables. The mean and total plant available water was greater in the distributed scenario in sand but not loamy sand (Figure 7). Greater lateral to vertical Darcy flow would lead to more root zone storage. In loamy sand, clustered I-SCMs resulted in the greatest ratios for lateral to vertical flow while both sand I-SCM arrangements produced the smallest ratios of lateral to vertical flow (Figure 10). The distributed loamy sand scenario produced ratios similar to sand during dry periods, but had a larger ratio during wet periods. This extreme difference between I-SCM arrangements in loamy sand as well as more saturated cells occurring under clustered I-SCMs (Figure 6b) led clustered I-SCMs to produce more plant available water than distributed I-SCMs.

Compared to sand, in loamy sand, clustered I-SCMs had more plant available water redistributed away from I-SCMs parallel to the stream, which is in some cases up an elevation gradient (Figure 7). This redistribution up an elevation gradient in the clustered I-SCMs in loamy sand resulted from a large saturated area leading to relatively large hydraulic conductivities and hydraulic gradients (Figure 7a and 7b).

Differences in plant available water between spatial arrangements in the same soil were much smaller than between soils. Loamy sand resulted in double the plant available water across the root zone than compared to sand. Shallower depth to water tables likely drove this difference, along with relationships between soil moisture and pressure-head (soil-moisture characteristic curves) where more water is in loamy sand soil than sand soil at the same pressure-head.

Cumulative plant available water within I-SCM sites was always greater in clustered compared to distributed I-SCMs. In sand, plant available water was very similar at I-SCMs since these cells never saturated in either case. In loamy sand plant available water was similar between spatial arrangements at I-SCMs during very dry times or during rainfall. During wet days I-SCMs reached saturation under both spatial arrangements and on very dry days moisture approached residual moisture under both spatial arrangements for loamy sand. After rainfall, distributed I-SCMs dried faster than clustered I-SCMs driving differences between the two to be larger. Clustered I-SCMs regularly held greater than 300 m^3 more water than distributed I-SCMs in loamy sand. These results suggest that clustered I-SCMs have greater potential to provide plants with substantial water over small areas compared to distributed I-SCMs. On the other hand, distributed I-SCMs have greater potential to provide water to plants over a larger area compared to I-SCMs, though the volume available will be less than that in the smaller area under clustered I-SCMs.

Sand had an aquifer diffusivity per aquifer thickness (Ds/b) six times larger than loamy sand (Table 1). After estimating aquifer thickness with average DTWT, aquifer diffusivity was still more than 4.8 times larger in sand than loamy sand. From the larger aquifer diffusivity for sand, we expected the response of baseflow in the sand to be more rapid to infiltrated water than loamy sand. Furthermore, response of baseflow to precipitation in sand was more dynamic in timing and magnitude than that observed in loamy sand.

Long term effect of I-SCM arrangement on baseflow magnitude was limited because we applied the same fluxes in each simulated scenario. This did not allow for soil moisture limited ET or other climatic feedbacks to be simulated and based on mass balance, if catchment inputs remain constant and simulations are run to steady-state, then outputs (discharge + ET) must be equal to inputs (precipitation). Since we applied ET as a consistent flux, steady-state discharges would be equal. While this limitation existed, by running transient simulations that were not at steady-state (annual inputs exceeded annual outputs) with consistent flux forcings between simulations we were able to make observations about rate of change of subsurface storage and discharge.

We hypothesized that focused, discrete spatial infiltration, when spatially distributed over larger areas, leads to larger lateral hydraulic gradients beneath I-SCMs resulting in significant lateral subsurface flow, decreasing episodic recharge and baseflow and increasing storage. Our distributed I-SCM arrangement did produce stronger lateral hydraulic gradients during precipitation events, but hydraulic conductivities were smaller with distributed I-SCMs and clustered I-SCMs maintained stronger lateral gradients during inter-event periods. This resulted in more lateral flow with clustered I-SCMs during all times except very dry periods where flow was small under both spatial arrangements (Figure 8). Distributed I-SCMs did lead to less recharge and increased storage, but this is attributed to greater average depth to water tables under distributed I-SCMs opposed to more lateral flow. We did not observe the hypothesized effect on baseflow. Long-term and episodic baseflow magnitudes were similar between spatial arrangements, but in sand, timing of baseflow response to precipitation was different (Figure 3g). Clustered I-SCMs delayed timing of peak baseflow response (Figure 5) and resulted in greater decrease of baseflow during interevent periods with low antecedent precipitation and smaller decreases, or even increases, in baseflow during interevent periods with high antecedent precipitation (Figure 4). This suggested relationships between I-SCM spatial arrangement and baseflow are more complex than our hypothesis suggested, and are dependent on antecedent moisture.

4.3 Alternative scenarios

Computational demand made simulating all possible combinations of alternative imperviousness, climate, and urban effects impossible. Our modeled system was a homogeneous isotropic alluvial headwater aquifer with extreme total imperviousness (98.5%) and extreme low effective imperviousness (0%). Less infiltrated stormwater would mute the baseflow response to I-SCMs, but we considered an extreme case such that the effect would be observable. Changes to total imperviousness would not have directly altered the model setup, because we defined effective imperviousness as 0% where all stormwater was routed to I-SCMs. If there were more pervious areas, however, ET occurring in these pervious areas could have removed soil moisture from the root zone, which would increase hydraulic gradients away from I-SCMs. Larger lateral hydraulic gradients away from I-SCMs would be expected to lead to greater unsaturated zone retention of infiltrated water, and decrease recharge and baseflow.

We simulated a moderately wet climate with below average ET to precipitation. With greater precipitation, the clustered scenario would become infeasible as groundwater mounding was already present in the loamy sand clustered scenario although this may be worked around by limiting capacity of surface storage at I-SCMs such that excess precipitation flows overland. Decreased ET would be expected to produce a similar effect as increased precipitation. Drier climates or climates with large annual ET would lend themselves to manipulating subsurface storage with I-SCM arrangement, but manipulating baseflow may be less feasible. We focused on the effect of spatial arrangement of I-SCMs, but there are many other factors that could affect urban subsurface storage and baseflow. Leaky infrastructure and water imports could increase baseflow. Larger distance from I-SCMs to the stream could mute the effect of infiltration on baseflow.

4.4 Management implications

Depending on management goals, different spatial arrangements of I-SCMs may be chosen. For example, in a Mediterranean climate with long dry periods between seasonal precipitation more distributed I-SCMs could be implemented to encourage greater retention of moisture in the unsaturated zone and subsurface. It can also be inferred that distributed I-SCMs in this scenario could further increase subsurface storage compared to clustered I-SCMs by increasing infiltration rates, by allowing some infiltration sites to be higher in elevation where there are likely greater depths to groundwater increasing infiltration rates compared to lower elevation infiltration sites. On the other hand, if management is in an arid climate where groundwater needs to be replenished clustered I-SCMs may be implemented to increase saturated storage.

In lower diffusivity soils, catchment discharge and storages may most effectively be altered by planting suitable vegetation in appropriate locations relative to locations of infiltration sites. While we acknowledge any vegetation planted in the ground will require at least a small area of perviousness, this area is not likely to experience the type of focused infiltration received at I-SCM locations. If there is only a small area where infiltration sites may be placed, or if they are already established in a clustered arrangement, then catchment outputs may be altered by planting appropriate vegetation within or very near the arranged I-SCMs which we expect to decrease long-term recharge and baseflow magnitude. On the other hand, if vegetation is desired, but recharge is favored over ET, then planting vegetation far away from the spatially clustered I-SCMs would be more appropriate. If only scattered (spatially distributed) small spaces are available for I-SCMs, then vegetation may be spread out over a larger area without decreasing ET, but if ET is not desired then vegetation would likely need to be placed up elevation gradient from I-SCMs. Conversely, in higher diffusivity soils vegetation may be less effective at altering recharge and baseflow since less water is retained in the root zone. These soils likely offer less opportunity to manage baseflow magnitude, but more opportunity to manage baseflow timing. The more dynamic rates of change of baseflow in the sand catchment support this hypothesis. As seen in Figures 4 and 5, I-SCMs arrangements magnified the relationship between antecedent precipitation and discharge in the sand catchment. If more consistent baseflow is desired (e.g. downstream water availability) in high diffusivity soils then distributed I-SCMs make more sense, but if more dynamic flow baseflow patterns are desired (e.g. biota needs occasional longer duration high flows) then more clustered I-SCMs would be the right choice.

Previous observational findings in a watershed developed with a distributed, high spatial density of infiltration SCMs, 0% effective imperviousness, and high diffusivity were that baseflow increased during development with reductions in ET (Bhaskar et al., 2016) the infiltrated stormwater moved rapidly to become recharge (Bhaskar et al., 2018). The reduction in ET during urban development is a common effect during urbanization, and alone would lead to increases in baseflow. Our work indicates that high diffusivity aquifers are not well suited to management of subsurface storage and baseflow magnitude with I-SCMs because infiltrated water quickly becomes recharge and moves through the aquifer. Instead, management of subsurface storage and baseflow magnitude in high diffusivity aquifers may counteract the reductions in ET with use of harvest based SCMs.

Chapter 5: Conclusions

Infiltration-based low impact development is an increasingly common approach to mitigating impacts of urbanization on streams and watershed-scale hydrologic function. We lacked a fundamental understanding of how spatial arrangement (clustered vs. distributed) of infiltration-based stormwater control measures (I-SCMs) affect subsurface storage and baseflow. To elucidate the relationship between I-SCM spatial arrangement, subsurface storage, and baseflow we used a fully distributed physically-based watershed model, ParFlow, to simulate two spatial arrangements of I-SCMs in two soils. We analyzed effects on catchment scale mass balance, partitioning of subsurface storage, discharge, and drivers of subsurface flow. Here we summarize findings related to our main research questions.

Question 1: How does spatial arrangement of I-SCMs affect total subsurface storage, partitioning of storage between unsaturated and saturated zones, and episodic baseflow recession and timing?

Results suggested distributed I-SCMs encourage greater unsaturated zone storage while clustered I-SCMs lead to greater saturated zone storage (Figures 3a, 3b, 3Ba, and 3Bb). Differences in unsaturated storage were larger than differences in saturated zone storage suggesting more distributed I-SCMs lead to increased total subsurface storage than more clustered I-SCMs. We showed that baseflow response to precipitation is manageable with I-SCM arrangements in high diffusivity aquifers, and in such cases, clustered I-SCMs produce delayed baseflow responses compared to distributed I-SCMs (Figures 3d, 3Bd, 4b and 5b). As antecedent precipitation decreases (drier times) clustered I-SCMs promote larger magnitude baseflow and as antecedent precipitation increases (wet times) distributed I-SCMs promote larger magnitude baseflow (Figure 3h).

Question 2: How are drivers of subsurface flow beneath infiltration facilities different between spatial arrangements?

Our modeled scenario suggested that during precipitation events, more distributed I-SCMs have larger lateral hydraulic gradients away from infiltration sites than more clustered I-SCMs (Figure 8b), whereas more clustered I-SCMs produce larger lateral hydraulic conductivities compared to more distributed arrangements (Figure 8a). Taking the product of these two factors, more clustered arrangements lead to larger lateral flow away from I-SCMs during rain events than more distributed arrangements, as larger hydraulic conductivities outweigh smaller hydraulic gradients (Figure 8c). Distributed I-SCMs produced greater vertical hydraulic gradients, similar vertical hydraulic conductivities, and greater vertical flow than clustered I-SCMs.

Question 3: How do the effects of spatial arrangement of I-SCMs on subsurface storage and baseflow vary among different soil types?

Results showed baseflow is more responsive to I-SCM spatial arrangement in high diffusivity aquifers (Figures 3d, 3Bd, 4 and 5) (e.g. sand) and subsurface storage and its partitioning between unsaturated and saturated zones are more responsive to I-SCM spatial arrangement in lower diffusivity aquifers (e.g., loamy sand).

Management implications of these findings for optimal spatial arrangement of infiltration-based stormwater control measures (I-SCMs) depend on management goals. Although infiltration of stormwater is sometimes thought of as water removal (i.e. out of sight out of mind), all stormwater infiltration is not equal. More spatially distributed arrangements of I-SCMs lead to longer-term retention of infiltrated water in the subsurface or availability of water in the unsaturated zone for plant uptake over larger areas. In contrast, if increased groundwater recharge is desired, then more clustered I-SCMs are preferable. In low permeability and low diffusivity aquifers, varying I-SCM arrangement is more likely to affect subsurface storage, including plant available water and partitioning between unsaturated and saturated zones, than baseflow. In such cases the best opportunity to manipulate subsurface storage to meet management goals is by altering locations of vegetation in relation to I-SCM location. In aquifers with very low infiltration capacity (e.g. silt), clustered I-SCMs are likely not possible and more distributed I-SCMs provide better opportunities to infiltrate stormwater. In extreme cases, large-scale infiltration of stormwater in very low permeability soils will lead to widespread groundwater mounding and surface ponding. High permeability aquifers offer less opportunity to manipulate catchment storage by I-SCM placement, but more opportunity to alter baseflow timing and recession behavior. In these aquifers if more consistent baseflow is desired (e.g. for downstream water supply) distributed I-SCMs are appropriate, but if more dynamic baseflow is desired (e.g. occasional longer duration high flows or low flows for fish rearing or recruitment) then clustered I-SCMs are better suited.

Unexplored interactions in this work include the effects of feedbacks between soil moisture, ET, I-SCM arrangement, and vegetation spatial arrangement. Exploring the role of vegetation in and near infiltration SCMs could be explored further by using a land surface model coupled to the watershed model.

References

Ashby, S F, and R D Falgout. 1996. "A P~arallel Multigrid Preconditioned Conjugate Gr~dient Algorithm for Groundwater Flow Simulations," 23.

Askarizadeh, Asal, Megan A. Rippy, Tim D. Fletcher, David L. Feldman, Jian Peng, Peter Bowler, Andrew S. Mehring, et al. 2015. "From Rain Tanks to Catchments: Use of Low-Impact Development To Address Hydrologic Symptoms of the Urban Stream Syndrome." *Environmental Science & Technology* 49 (19): 11264–80. https://doi.org/10.1021/acs.est.5b01635.

Barnes, Michael L., Claire Welty, and Andrew J. Miller. 2016. "Global Topographic Slope Enforcement to Ensure Connectivity and Drainage in an Urban Terrain." *Journal of Hydrologic Engineering* 21 (4): 06015017. https://doi.org/10.1061/(ASCE)HE.1943-5584.0001306.

Bhaskar, Aditi S., L. Beesley, M. J. Burns, T. D. Fletcher, P. Hamel, C. E. Oldham, and A. H. Roy. 2016. "Will It Rise or Will It Fall? Managing the Complex Effects of Urbanization on Base Flow." *Freshwater Science* 35 (1): 293–310. https://doi.org/10.1086/685084.

Bhaskar, Aditi S., Dianna M. Hogan, and Stacey A. Archfield. 2016. "Urban Base Flow with Low Impact Development: Urban Base Flow with Low Impact Development." *Hydrological Processes* 30 (18): 3156–71. https://doi.org/10.1002/hyp.10808.

Bhaskar, Aditi S., Dianna M. Hogan, John R. Nimmo, and Kimberlie S. Perkins. 2018. "Groundwater Recharge amidst Focused Stormwater Infiltration." *Hydrological Processes* 32 (13): 2058–68. https://doi.org/10.1002/hyp.13137.

Bhaskar, Aditi S., Claire Welty, Reed M. Maxwell, and Andrew J. Miller. 2015. "Untangling the Effects of Urban Development on Subsurface Storage in Baltimore." *Water Resources Research* 51 (2): 1158–81. https://doi.org/10.1002/2014WR016039.

Chui, Ting Fong May, and Dieu Huong Trinh. 2016. "Modelling Infiltration Enhancement in a Tropical Urban Catchment for Improved Stormwater Management: Infiltration Enhancement in a Tropical Urban Catchment." *Hydrological Processes*. https://doi.org/10.1002/hyp.10926.

Eger, Caitlin G., David G. Chandler, and Charles T. Driscoll. 2017. "Hydrologic Processes That Govern Stormwater Infrastructure Behaviour." *Hydrological Processes* 31 (25): 4492–4506. https://doi.org/10.1002/hyp.11353.

Endreny, T., and V. Collins. 2009. "Implications of Bioretention Basin Spatial Arrangements on Stormwater Recharge and Groundwater Mounding." *Ecological Engineering* 35 (5): 670–77. https://doi.org/10.1016/j.ecoleng.2008.10.017.

Genuchten, M. Th. van. 1980. "A Closed-Form Equation for Predicting the Hydraulic Conductivity of Unsaturated Soils1." *Soil Science Society of America Journal* 44 (5): 892. https://doi.org/10.2136/sssaj1980.03615995004400050002x.

Gilroy, Kristin L., and Richard H. McCuen. 2009. "Spatio-Temporal Effects of Low Impact Development Practices." *Journal of Hydrology* 367 (3–4): 228–36. https://doi.org/10.1016/j.jhydrol.2009.01.008.

Göbel, Patricia, Holger Stubbe, Mareike Weinert, Julia Zimmermann, Stefan Fach, Carsten Dierkes, Holger Kories, et al. 2004. "Near-Natural Stormwater Management and Its Effects on the Water Budget and Groundwater Surface in Urban Areas Taking Account of the Hydrogeological Conditions." *Journal of Hydrology* 299 (3–4): 267–83. https://doi.org/10.1016/j.jhydrol.2004.08.013.

Gupta, Satish, Amanjot Singh, and Andry Ranaivoson. 2004. "Moisture Retention Characteristics of Base and Sub-Base Materials."

Hamel, Perrine, Edoardo Daly, and Tim D. Fletcher. 2013. "Source-Control Stormwater Management for Mitigating the Impacts of Urbanisation on Baseflow: A Review." *Journal of Hydrology* 485 (April): 201–11. https://doi.org/10.1016/j.jhydrol.2013.01.001.

Hamel, Perrine, and Tim D. Fletcher. 2014. "Modelling the Impact of Stormwater Source Control Infiltration Techniques on Catchment Baseflow." *Hydrological Processes* 28 (24): 5817–31. https://doi.org/10.1002/hyp.10069.

Healy, Richard W. 2010. *Estimating Groundwater Recharge*. 1st ed. Cambridge University Press.

Heber Green, W., and G. A. Ampt. 1911. "Studies on Soil Phyics." *The Journal of Agricultural Science* 4 (1): 1–24. https://doi.org/10.1017/S0021859600001441.

Hood, Mark J., John C. Clausen, and Glenn S. Warner. 2007. "Comparison of Stormwater Lag Times for Low Impact and Traditional Residential Development." *Journal of the American Water Resources Association* 43 (4): 1036–46. https://doi.org/10.1111/j.1752-1688.2007.00085.x.

James, Matthew B., and Randel L. Dymond. 2012. "Bioretention Hydrologic Performance in an Urban Stormwater Network." *Journal of Hydrologic Engineering* 17 (3): 431–36. https://doi.org/10.1061/(ASCE)HE.1943-5584.0000448.

Jefferson, Anne J., Aditi S. Bhaskar, Kristina G. Hopkins, Rosemary Fanelli, Pedro M. Avellaneda, and Sara K. McMillan. 2017. "Stormwater Management Network Effectiveness and Implications for Urban Watershed Function: A Critical Review." *Hydrological Processes* 31 (23): 4056–80. https://doi.org/10.1002/hyp.11347.

Jones, Jim E, and Carol S Woodward. 2001. "Newton±Krylov-Multigrid Solvers for Large-Scale, Highly Heterogeneous, Variably Saturated ¯ow Problems Q." *Advances in Water Resources*, 12.

Kollet, Stefan J., and Reed M. Maxwell. 2006. "Integrated Surface–Groundwater Flow Modeling: A Free-Surface Overland Flow Boundary Condition in a Parallel Groundwater Flow Model." *Advances in Water Resources* 29 (7): 945–58. https://doi.org/10.1016/j.advwatres.2005.08.006.

Lerner, David N. 2002. "Identifying and Quantifying Urban Recharge: A Review." *Hydrogeology Journal* 10 (1): 143–52. https://doi.org/10.1007/s10040-001-0177-1.

Li, Congying, Tim D. Fletcher, Hugh P. Duncan, and Matthew J. Burns. 2017. "Can Stormwater Control Measures Restore Altered Urban Flow Regimes at the Catchment Scale?" *Journal of Hydrology* 549 (June): 631–53. https://doi.org/10.1016/j.jhydrol.2017.03.037.

Lim, Theodore C, and Claire Welty. 2017. "Effects of Spatial Configuration of Imperviousness and Green Infrastructure Networks on Hydrologic Response in a Residential Sewershed: SPATIAL GREEN INFRASTRUCTURE NETWORKS." *Water Resources Research* 53 (9): 8084–8104. https://doi.org/10.1002/2017WR020631.

Loperfido, J.V., Gregory B. Noe, S. Taylor Jarnagin, and Dianna M. Hogan. 2014. "Effects of Distributed and Centralized Stormwater Best Management Practices and Land Cover on Urban Stream Hydrology at the Catchment Scale." *Journal of Hydrology* 519 (November): 2584–95. https://doi.org/10.1016/j.jhydrol.2014.07.007.

Maxwell, Reed M. 2013. "A Terrain-Following Grid Transform and Preconditioner for Parallel, Large-Scale, Integrated Hydrologic Modeling." *Advances in Water Resources* 53 (March): 109–17. https://doi.org/10.1016/j.advwatres.2012.10.001.

Miles, Brian, and Lawrence E. Band. 2015. "Green Infrastructure Stormwater Management at the Watershed Scale: Urban Variable Source Area and Watershed Capacitance: INVITED COMMENTARY." *Hydrological Processes* 29 (9): 2268–74. https://doi.org/10.1002/hyp.10448.

Newcomer, Michelle E., Jason J. Gurdak, Leonard S. Sklar, and Leora Nanus. 2014. "Urban Recharge beneath Low Impact Development and Effects of Climate Variability and Change: RECHARGE BENEATH LOW IMPACT DEVELOPMENT AND CLIMATE CHANGE." *Water Resources Research* 50 (2): 1716–34. https://doi.org/10.1002/2013WR014282.

Poff, N. LeRoy, J. David Allan, Mark B. Bain, James R. Karr, Karen L. Prestegaard, Brian D. Richter, Richard E. Sparks, and Julie C. Stromberg. 1997. "The Natural Flow Regime." *BioScience* 47 (11): 769–84. https://doi.org/10.2307/1313099.

Price, Katie. 2011. "Effects of Watershed Topography, Soils, Land Use, and Climate on Baseflow Hydrology in Humid Regions: A Review." *Progress in Physical Geography* 35 (4): 465–92. https://doi.org/10.1177/0309133311402714.

Rossman, Lewis A. 2015. "Storm Water Management Model User's Manual Version 5.1," 353.

Schaap, Marcel G., Feike J. Leij, and Martinus Th. van Genuchten. 2001. “Rosetta : A Computer Program for Estimating Soil Hydraulic Parameters with Hierarchical Pedotransfer Functions.” *Journal of Hydrology* 251 (3–4): 163–76. https://doi.org/10.1016/S0022-1694(01)00466-8.

Seck, Alimatou, Claire Welty, and Reed M. Maxwell. 2015. “Spin-up Behavior and Effects of Initial Conditions for an Integrated Hydrologic Model: Spin-up Behavior and Effects of Initial Conditions.” *Water Resources Research* 51 (4): 2188–2210. https://doi.org/10.1002/2014WR016371.

Staudinger, Maria, Michael Stoelzle, Fabien Cochand, Jan Seibert, Markus Weiler, and Daniel Hunkeler. 2019. “Your Work Is My Boundary Condition!” *Journal of Hydrology* 571 (April): 235–43. https://doi.org/10.1016/j.jhydrol.2019.01.058.

Thomas, Brian, Ali Behrangi, and James Famiglietti. 2016. “Precipitation Intensity Effects on Groundwater Recharge in the Southwestern United States.” *Water* 8 (3): 90. https://doi.org/10.3390/w8030090.

Walsh, Christopher J, Allison H Roy, Jack W Feminella, Peter D Cottingham, and Peter M Groffman. 2005. “The Urban Stream Syndrome: Current Knowledge and the Search for a Cure” 24: 18.

Wiles, Thomas J., and John M. Sharp Jr. 2008. “The Secondary Permeability of Impervious Cover.” *Environmental & Engineering Geoscience* 14 (4): 251–65.

Woods, Ross A., Murugesu Sivapalan, and Justin S. Robinson. 1997. “Modeling the Spatial Variability of Subsurface Runoff Using a Topographic Index.” *Water Resources Research* 33 (5): 1061–73. https://doi.org/10.1029/97WR00232.